

# Mutual Information-Maximizing Quantized Belief Propagation Decoding of LDPC Codes

Xuan He, Kui Cai, and Zhen Mei

**Abstract**—A severe problem for mutual information-maximizing lookup table (MIM-LUT) decoding of low-density parity-check (LDPC) code is the high memory cost for using large tables, while decomposing large tables to small tables deteriorates decoding error performance. In this paper, we propose a method, called mutual information-maximizing quantized belief propagation (MIM-QBP) decoding, to remove the lookup tables used for MIM-LUT decoding. Our method leads to a very practical decoder, namely MIM-QBP decoder, which can be implemented based only on simple mappings and fixed-point additions. We further present how to practically and systematically design the MIM-QBP decoder for both regular and irregular LDPC codes. Simulation results show that the MIM-QBP decoder can always considerably outperform the state-of-the-art MIM-LUT decoder. Furthermore, the MIM-QBP decoder with only 3 bits per message can outperform the floating-point belief propagation (BP) decoder at high signal-to-noise ratio (SNR) region when testing on high rate codes with a maximum of 10–30 iterations.

**Index Terms**—Finite alphabet iterative decoding (FAID), lookup table (LUT), low-density parity-check (LDPC) code, mutual information (MI), quantized belief propagation (QBP).

## I. INTRODUCTION

Low-density parity-check (LDPC) codes [1] have been widely applied to communication and data storage systems due to their capacity approaching performance. For the sake of simple hardware implementation, many efforts have been devoted to efficiently represent messages for LDPC decoding [2]–[14]. Among them, Chen *et al.* [2] approximated the belief propagation (BP) algorithm by representing log-likelihood ratios (LLRs) with a low resolution, generally 5 to 7 bits. The works in [3]–[14] focused on finite alphabet iterative decoding (FAID), which makes use of messages represented by symbols from finite alphabets instead of messages represented by LLRs. FAID algorithms with messages represented by 3 to 4 bits can approach the floating-point BP algorithm within 0.2 dB [3]–[14].

Non-uniform quantized BP (QBP) algorithms were investigated in [4]–[6], where a decoder was implemented based on simple mappings and additions (including subtractions). However, since only the decoding of the (3, 6) LDPC code (code with variable node (VN) degree 3 and check node (CN) degree 6) was considered and significant amount of hand optimization was needed for the decoder design [4]–[6], we can hardly generalize the design to a different scenario.

Recently, mutual information-maximizing lookup table (MIM-LUT) decoding was considered in [7]–[14], among which [13] and [14] focused on the decoding of irregular LDPC codes. An MIM-LUT decoder can reduce the hardware

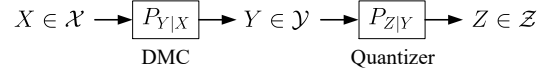


Fig. 1. Quantization of a discrete memoryless channel (DMC).

complexity and increase the decoding throughput. However, a serious problem on the memory requirement may arise when the sizes of the lookup tables (LUTs) are large. To avoid this problem, these tables were decomposed to small tables at the cost of deteriorating the decoder's error performance [7]–[14].

In this paper, we propose a method, called mutual information-maximizing quantized belief propagation (MIM-QBP) decoding, to remove the tables used for MIM-LUT decoding [7]–[14] so as to greatly save memory costs. Our method leads to a hardware-friendly decoder, namely, the MIM-QBP decoder, which can be implemented based only on simple mappings and fixed-point additions (including subtractions). From this point of view, our decoder works similarly to those presented by [4]–[6], but instead of using hand optimization, we show how to practically and systematically design the MIM-QBP decoder for both regular and irregular LDPC codes. Simulation results show that the MIM-QBP decoder can always considerably outperform the state-of-the-art MIM-LUT decoder [7]–[14]. Moreover, the MIM-QBP decoder with only 3 bits per message can outperform the floating-point BP decoder at high signal-to-noise ratio (SNR) region when testing on high rate codes with a maximum of 10–30 iterations.

The remainder of this paper is organized as follows. Section II first introduces the optimal quantization method for binary-input discrete memoryless channel (DMC), and then gives a review of the MIM-LUT decoding and also highlights the linkage between the two topics. Section III shows the necessity for removing the tables used for MIM-LUT decoding, and then proposes the MIM-QBP decoding for regular LDPC codes. Section IV presents how to practically design the MIM-QBP decoder. Section V illustrates the design of MIM-QBP decoder for irregular LDPC codes. Section VI presents the simulation results. Finally, Section VII concludes this paper.

## II. PRELIMINARIES

### A. Mutual Information-Maximizing Quantization of Binary-Input DMC

Consider the quantization of a binary-input DMC as shown by Fig. 1. The channel input  $X$  takes values from  $\mathcal{X} = \{0, 1\}$  with probability  $P_X(0)$  and  $P_X(1)$ , respectively. The

channel output  $Y$  takes values from  $\mathcal{Y} = \{y_1, y_2, \dots, y_N\}$  with channel transition probability given by  $P_{Y|X}(y_j|x) = \Pr(Y = y_j|X = x)$ , where  $x = 0, 1$  and  $j = 1, 2, \dots, N$ . The channel output  $Y$  is quantized to  $Z$  which takes values from  $\mathcal{Z} = \{1, 2, \dots, M\}$ . A well-known criterion for channel quantization [15], [16] is to design a quantizer  $Q^* : \mathcal{Y} \rightarrow \mathcal{Z}$  to maximize the mutual information (MI) between  $X$  and  $Z$ , i.e.

$$Q^* = \arg \max_Q I(X; Z) \\ = \arg \max_Q \sum_{x \in \mathcal{X}, z \in \mathcal{Z}} P_{X,Z}(x, z) \log \frac{P_{X,Z}(x, z)}{P_X(x)P_Z(z)}, \quad (1)$$

where  $P_{X,Z}(x, z) = P_X(x) \sum_{y \in \mathcal{Y}} P_{Y|X}(y|x) P_{Z|Y}(z|y)$  and  $P_Z(z) = \sum_{x \in \mathcal{X}} P_{X,Z}(x, z)$ .

A deterministic quantizer (DQ)  $Q : \mathcal{Y} \rightarrow \mathcal{Z}$  means that for each  $y \in \mathcal{Y}$ , there exists a unique  $z \in \mathcal{Z}$  such that  $P_{Z|Y}(z|y) = 1$  and  $P_{Z|Y}(z'|y) = 0$  for  $z \neq z' \in \mathcal{Z}$ . Let  $Q^{-1}(z) \subset \mathcal{Y}$  denote the preimage of  $z \in \mathcal{Z}$ . We name  $Q$  a sequential deterministic quantizer (SDQ) [16] if it can be equivalently described by an integer set  $\Lambda = \{\lambda_0, \lambda_1, \dots, \lambda_{M-1}, \lambda_M\}$  with  $\lambda_0 = 0 < \lambda_1 < \dots < \lambda_{M-1} < \lambda_M = N$  in the way below

$$\begin{cases} Q^{-1}(1) = \{y_1, y_2, \dots, y_{\lambda_1}\}, \\ Q^{-1}(2) = \{y_{\lambda_1+1}, y_{\lambda_1+2}, \dots, y_{\lambda_2}\}, \\ \vdots \\ Q^{-1}(M) = \{y_{\lambda_{M-1}+1}, y_{\lambda_{M-1}+2}, \dots, y_{\lambda_M}\}. \end{cases}$$

We thus also name  $\Lambda$  an SDQ.

According to [15],  $Q^*$  in (1) must be deterministic; meanwhile,  $Q^*$  is an optimal SDQ when elements in  $\mathcal{Y}$  are relabelled to satisfy

$$\frac{P_{Y|X}(y_1|0)}{P_{Y|X}(y_1|1)} \geq \frac{P_{Y|X}(y_2|0)}{P_{Y|X}(y_2|1)} \geq \dots \geq \frac{P_{Y|X}(y_N|0)}{P_{Y|X}(y_N|1)}. \quad (2)$$

Note that after merging any two elements  $y, y' \in \mathcal{Y}$  with  $P_{Y|X}(y|0)/P_{Y|X}(y|1) = P_{Y|X}(y'|0)/P_{Y|X}(y'|1)$ , the resulting optimal quantizer is as optimal as the original one [15]. A method based on dynamic programming (DP) [17, Section 15.3] was proposed in [15] to find  $Q^*$  with complexity  $O((N - M)^2 M)$ . Moreover, a general framework has been developed in [16] for applying DP to find an optimal SDQ  $\Lambda^*$  to maximize  $I(X; Z)$  for cases that the labeling of the elements in  $\mathcal{Y}$  is fixed and  $\Lambda^*$  is an SDQ.

The quantization model in Fig. 1 can be used to quantize the binary-input continuous memoryless channel, such as quantizing the binary-input additive white Gaussian noise (AWGN) channel. This task can be done by first uniformly quantizing the AWGN channel to a DMC with  $N$  outputs, where  $N \gg M$ . Then, the quantization model in Fig. 1 is applicable. If we use an SDQ to implement the quantization, the SDQ can be equivalently described by  $M - 1$  thresholds  $\{\tau_1, \tau_2, \dots, \tau_{M-1}\}$  with  $\tau_1 < \tau_2 < \dots < \tau_{M-1}$ , such that for

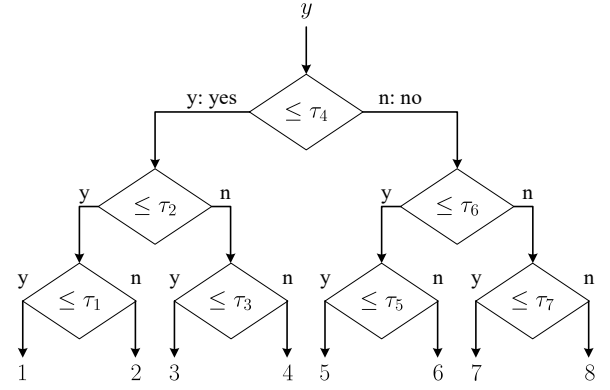


Fig. 2. Binary search tree-like structure for implementing the quantization of additive white Gaussian noise (AWGN) channel, where the quantization threshold set is  $\{\tau_1, \tau_2, \dots, \tau_{M-1}\}$  with  $\tau_1 < \tau_2 < \dots < \tau_{M-1}$  and quantization output alphabet is  $\{1, 2, \dots, 8\}$ .

any continuous channel output  $y \in \mathbb{R}$ , its quantization output  $\tilde{y}$  is given by

$$\tilde{y} = \begin{cases} 1 & y \leq \tau_1, \\ M & y > \tau_{M-1}, \\ i & \tau_{i-1} < y \leq \tau_i, 1 < i < M. \end{cases} \quad (3)$$

More details can be found in [16]. Given  $\{\tau_1, \tau_2, \dots, \tau_{M-1}\}$ , implementing the quantization in (3) has complexity  $O(\lceil \log_2(M) \rceil)$ , which is illustrated by Fig. 2 for  $M = 8$ .

### B. MIM-LUT Decoder Design for Regular LDPC Codes

Consider a binary-input DMC. Denote the channel input by  $X$  which takes values from  $\mathcal{X} = \{0, 1\}$  with equal probability, i.e.,  $P_X(0) = P_X(1) = 1/2$ . Denote  $L$  as the DMC output which takes values from  $\mathcal{L} = \{0, 1, \dots, |\mathcal{L}| - 1\}$  with channel transition probability  $P_{L|X}$ . By using the quantization method introduced in Section II-A, we can set  $|\mathcal{L}|$  according to our needs for different decoding iterations.

Consider to design a quantized message passing (MP) decoder for a regular  $(d_v, d_c)$  LDPC code. Denote  $\mathcal{R} = \{0, 1, \dots, |\mathcal{R}| - 1\}$  and  $\mathcal{S} = \{0, 1, \dots, |\mathcal{S}| - 1\}$  as the alphabets of messages passed from VN to CN and vice versa. Note that  $\mathcal{L}, \mathcal{R}, \mathcal{S}$  and their related notations may or may not vary with iterations. We have used these notations without specifying their associated iterations, because after specifying the decoder design for one iteration, the design is clear for all iterations.

For the message  $R \in \mathcal{R}$  (resp.  $S \in \mathcal{S}$ ) passed from VN to CN (resp. CN to VN), we use  $P_{R|X}$  (resp.  $P_{S|X}$ ) to denote the probability mass function (pmf) of  $R$  (resp.  $S$ ) conditioned on the channel input bit  $X$ . If the code graph is cycle-free,  $R$  (resp.  $S$ ) conditioned on  $X$  is independent and identically distributed (i.i.d.) with respect to different edges at a same iteration. The design of the MIM-LUT decoder [7]–[14] is carried out by using density evolution [4], [18] (by tracing  $P_{R|X}$  and  $P_{S|X}$ ) over the assumption of cycle-free code graph. However, the MIM-LUT decoder can work well on code graphs containing cycles.

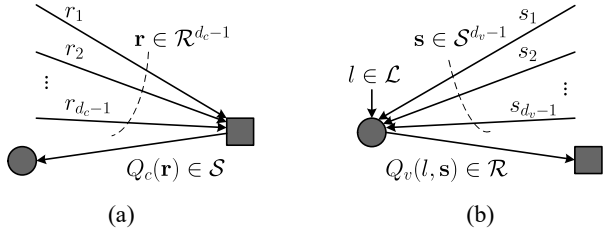


Fig. 3. Node update for mutual information-maximizing lookup table (MIM-LUT) decoding, where the circle and square represent a variable and check node, respectively. (a) Check node update. (b) Variable node update.

For each iteration, design of the update function (UF)

$$Q_c : \mathcal{R}^{d_c-1} \rightarrow \mathcal{S} \quad (4)$$

for CN update comes first, where the CN update is shown by Fig. 3(a). The MIM-LUT decoding methods design  $Q_c$  to maximize  $I(X; S)$ . For easily understanding this design problem, we can equivalently convert it to the problem of DMC quantization, as shown by Fig. 4.

We assume  $P_{R|X}$  is known, because for the first iteration,  $P_{R|X}$  can be solely derived from the channel transition probability  $P_{L|X}$ , and for the other iteration,  $P_{R|X}$  is known after the design at VN is completed. The joint distribution  $P_{\mathbf{R}|X}$  of the incoming message  $\mathbf{R} \in \mathcal{R}^{d_c-1}$  conditioned on the channel input bit  $X$  at a CN (i.e., the channel transition probability  $P_{\mathbf{R}|X}$  with respect to the DMC shown by Fig. 4) is given by [9]

$$P_{\mathbf{R}|X}(\mathbf{r}|x) = \left(\frac{1}{2}\right)^{\dim(\mathbf{r})-1} \sum_{\mathbf{x}:\oplus \mathbf{x}=x} \prod_{i=1}^{\dim(\mathbf{r})} P_{R_i|X}(r_i|x_i), \quad (5)$$

where  $\mathbf{r} = (r_1, r_2, \dots, r_{d_c-1}) \in \mathcal{R}^{d_c-1}$  is a realization of  $\mathbf{R}$ ,  $\dim(\mathbf{r}) = d_c - 1$  is the dimension of  $\mathbf{r}$ ,  $x \in \mathcal{X}$  is a realization of  $X$ ,  $\mathbf{x} = (x_1, x_2, \dots, x_{d_c-1}) \in \mathcal{X}^{d_c-1}$  consists of channel input bits corresponding to the VNs associated with incoming edges,  $\oplus \mathbf{x} = x_1 \oplus x_2 \oplus \dots \oplus x_{d_c-1}$  with  $\oplus$  denoting the addition in  $GF(2)$ . Based on (5), we have

$$\begin{cases} P_{\mathbf{R}|X}(\mathbf{r}|0) \pm P_{\mathbf{R}|X}(\mathbf{r}|1) = \left(\frac{1}{2}\right)^{\dim(\mathbf{r})-1} \cdot \prod_{i=1}^{\dim(\mathbf{r})} (P_{R_i|X}(r_i|0) \pm P_{R_i|X}(r_i|1)), \\ P_{X|\mathbf{R}}(0|\mathbf{r}) \pm P_{X|\mathbf{R}}(1|\mathbf{r}) = \prod_{i=1}^{\dim(\mathbf{r})} (P_{X|R_i}(0|r_i) \pm P_{X|R_i}(1|r_i)). \end{cases} \quad (6)$$

Given  $P_{\mathbf{R}|X}$ , the design of  $Q_c$  is equivalent to the design of  $Q^*$  in (1) by setting  $\mathcal{Y} = \mathcal{R}^{d_c-1}$  and  $\mathcal{Z} = \mathcal{S}$ . We can solve this design problem by using the DP method proposed in [15], after listing  $\mathbf{r}$  in descending order based on  $P_{\mathbf{R}|X}(\mathbf{r}|0)/P_{\mathbf{R}|X}(\mathbf{r}|1)$  (see (2)). After the design of  $Q_c$ , a LUT is typically used for storing  $Q_c$ , and the output message  $S$  is passed to the CN's neighbour VNs with  $P_{S|X}$  given by

$$P_{S|X}(s|x) = \sum_{\mathbf{r} \in Q_c^{-1}(s)} P_{\mathbf{R}|X}(\mathbf{r}|x). \quad (7)$$

Then, design of the UF

$$Q_v : \mathcal{L} \times \mathcal{S}^{d_v-1} \rightarrow \mathcal{R} \quad (8)$$

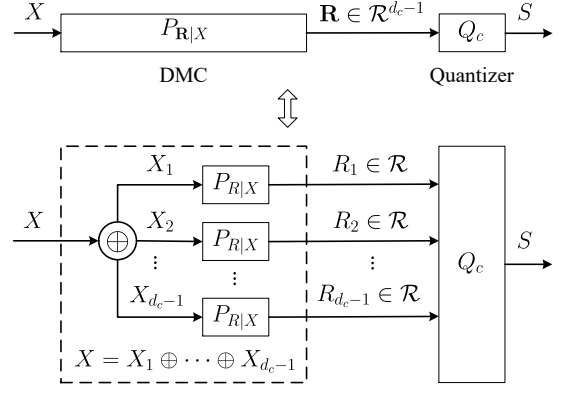


Fig. 4. Quantization of a discrete memoryless channel (DMC), where the quantizer works exactly the same as the check node update function  $Q_c$  for the mutual information-maximizing lookup table (MIM-LUT) decoding shown by Fig. 3(a).

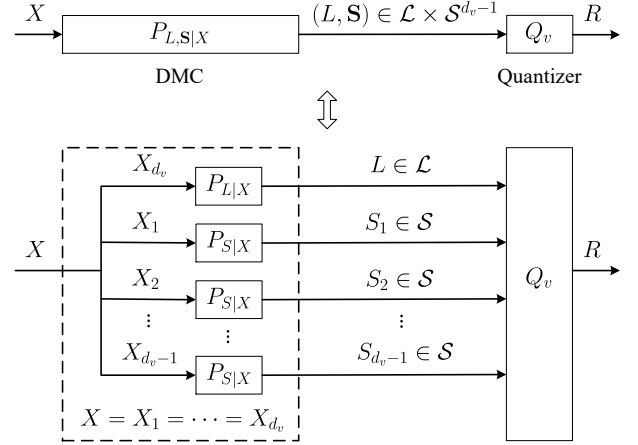


Fig. 5. Quantization of a discrete memoryless channel (DMC), where the quantizer works exactly the same as the variable node update function  $Q_v$  for the mutual information-maximizing lookup table (MIM-LUT) decoding shown by Fig. 3(b).

for VN update starts, where the VN update is shown by Fig. 3(b). The MIM-LUT decoding methods also design  $Q_v$  to maximize  $I(X; R)$ . For easily understanding this design problem, we can equivalently convert it to the problem of DMC quantization, as shown by Fig. 5.

The joint distribution  $P_{L,S|X}$  of incoming message  $(L, \mathbf{S}) \in \mathcal{L} \times \mathcal{S}^{d_v-1}$  conditioned on the channel input bit  $X$  at a VN (i.e., the channel transition probability  $P_{L,S|X}$  with respect to the DMC shown by Fig. 5) is given by [9]

$$P_{L,S|X}(l, \mathbf{s}|x) = P_{L|X}(l|x) \prod_{i=1}^{\dim(\mathbf{s})} P_{S_i|X}(s_i|x), \quad (9)$$

where  $l \in \mathcal{L}$  is a realization of  $L$ ,  $\mathbf{s} = (s_1, s_2, \dots, s_{d_v-1}) \in \mathcal{S}^{d_v-1}$  is a realization of  $\mathbf{S}$ ,  $\dim(\mathbf{s}) = d_v - 1$  is the dimension of  $\mathbf{s}$ , and  $x \in \mathcal{X}$  is a realization of  $X$ .

Given  $P_{L,S|X}$ , the design of  $Q_v$  is equivalent to the design of  $Q^*$  in (1) by setting  $\mathcal{Y} = \mathcal{L} \times \mathcal{S}^{d_v-1}$  and  $\mathcal{Z} = \mathcal{R}$ . We can solve this design problem by using the DP method

proposed in [15], after listing  $(l, s)$  in descending order based on  $P_{L,S|X}(l, s|0)/P_{L,S|X}(l, s|1)$  (see (2)). After the design of  $Q_v$ , a LUT is typically used for storing  $Q_v$ , and the output message  $R$  is passed to the VN's neighbour CNs with  $P_{R|X}$  given by

$$P_{R|X}(r|x) = \sum_{(l,s) \in Q_v^{-1}(r)} P_{L,S|X}(l, s|x). \quad (10)$$

For each iteration, we can design the estimation function

$$Q_e : \mathcal{L} \times \mathcal{S}^{d_v} \rightarrow \mathcal{X} \quad (11)$$

to estimate the channel input bit corresponding to each VN. The design can be carried out similarly to the design of  $Q_v$ . The two main differences involved in the design are that i) the incoming message alphabet  $\mathcal{L} \times \mathcal{S}^{d_v-1}$  is changed to  $\mathcal{L} \times \mathcal{S}^{d_v}$  and ii) the outgoing message alphabet  $\mathcal{R}$  is changed to  $\mathcal{X}$ . Therefore, we ignore the details.

After finishing the design of  $Q_c$ ,  $Q_v$ , and  $Q_e$  for all iterations, the design of the MIM-LUT decoder is completed. In general,  $|\mathcal{L}| = |\mathcal{R}| = |\mathcal{S}| = 8$  (resp. 16) is used for all iterations, leading to a 3-bit (resp. 4-bit) decoder. Given  $|\mathcal{L}|, |\mathcal{R}|, |\mathcal{S}|$ , and the maximum allowed decoding iterations, the quality of the MIM-LUT decoder heavily depends on the choice of  $P_{L|X}$ , which is essentially determined by the design noise standard derivation  $\sigma_d$ . The maximum noise standard derivation  $\sigma^*$ , which can make  $I(X; R)$  approach 1 after reaching the maximum decoding iteration, is called the decoding threshold. Empirically, a good  $\sigma_d$  should be around  $\sigma^*$  as investigated in [7]–[14].

### III. MIM-QBP DECODING OF REGULAR LDPC CODES

#### A. Motivation

When implementing MIM-LUT decoding,  $Q_c$ ,  $Q_v$ , and  $Q_e$  are implemented by using LUTs, and then the decoding works efficiently by using table lookup. The sizes of tables for implementing  $Q_c$ ,  $Q_v$ , and  $Q_e$  are  $|\mathcal{R}|^{d_c-1}$ ,  $|\mathcal{L}| \cdot |\mathcal{S}|^{d_v-1}$ , and  $|\mathcal{L}| \cdot |\mathcal{S}|^{d_v}$ , respectively. Thus, a serious problem for a very large memory requirement may arise due to these tables' large sizes in practice. To solve this problem, current MIM-LUT decoding methods [7]–[14] decompose  $Q_c$ ,  $Q_v$ , and  $Q_e$  into a series of subfunctions, each working on two incoming messages. After this decomposition, the sizes of tables for implementing  $Q_c$ ,  $Q_v$ , and  $Q_e$  are reduced to  $(d_c - 2)|\mathcal{R}|^2$ ,  $(d_v - 2)|\mathcal{S}|^2 + |\mathcal{L}||\mathcal{S}|$ , and  $(d_v - 1)|\mathcal{S}|^2 + |\mathcal{L}||\mathcal{S}|$ , respectively. This decomposition technique can significantly reduce the cost for storage, but at the same time, will degrade the performance of  $Q_c$ ,  $Q_v$ , and  $Q_e$  in terms of maximizing MI, as shown in the example below.

*Example 1:* Consider the UF  $Q_v : \mathcal{L} \times \mathcal{S}^2 \rightarrow \mathcal{R}$  at a VN (i.e.,  $d_v = 3$ ). Assume that  $\mathcal{L} = \mathcal{S} = \mathcal{R} = \{0, 1\}$  and the conditional probabilities  $P_{L|X}$  and  $P_{S|X}$  are given by

$$P_{L|X}(l|x) = \begin{cases} 3/4 & l = x, \\ 1/4 & l \neq x, \end{cases} \quad (12)$$

TABLE I  
JOINT DISTRIBUTION  $P_{L,S_1,S_2|X}$  AND THE OPTIMAL QUANTIZER  $Q_v$ ,  
WHERE  $(l, s_1, s_2)$  IS LISTED IN DESCENDING ORDER FROM TOP TO  
BOTTOM BASED ON  $P_{L,S_1,S_2|X}(\cdot|0)/P_{L,S_1,S_2|X}(\cdot|1)$

$(l, s_1, s_2)$	$P_{L,S_1,S_2 X}(\cdot 0)$	$P_{L,S_1,S_2 X}(\cdot 1)$	$Q_v(\cdot)$
(0, 0, 0)	12/36	1/36	0
(0, 0, 1)	6/36	2/36	0
(0, 1, 0)	6/36	2/36	0
(1, 0, 0)	4/36	3/36	0
(0, 1, 1)	3/36	4/36	1
(1, 0, 1)	2/36	6/36	1
(1, 1, 0)	2/36	6/36	1
(1, 1, 1)	1/36	12/36	1

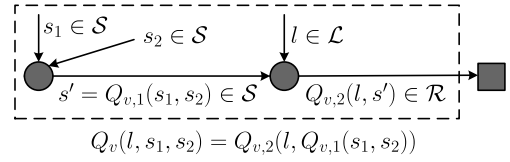


Fig. 6. Decomposing  $Q_v : \mathcal{L} \times \mathcal{S}^2 \rightarrow \mathcal{R}$  into two subfunctions  $Q_{v,1} : \mathcal{S}^2 \rightarrow \mathcal{S}$  and  $Q_{v,2} : \mathcal{L} \times \mathcal{S} \rightarrow \mathcal{R}$  in the way of  $Q_v(l, s_1, s_2) = Q_{v,2}(l, Q_{v,1}(s_1, s_2))$ .

and

$$P_{S|X}(s|x) = \begin{cases} 2/3 & s = x, \\ 1/3 & s \neq x, \end{cases} \quad (13)$$

respectively. Based on (9), the joint distribution  $P_{L,S_1,S_2|X}$ , with  $L$  from channel and  $(S_1, S_2)$  from CN, is given by Table I.  $Q_v$  is an MIM quantizer (in the sense that  $(L, S_1, S_2)$  is the input message) maximizing  $I(X; R)$  with  $I(X; R) = 0.236$ .

We now consider to decompose  $Q_v$  into two subfunctions  $Q_{v,1} : \mathcal{S}^2 \rightarrow \mathcal{S}$  and  $Q_{v,2} : \mathcal{L} \times \mathcal{S} \rightarrow \mathcal{R}$ , as shown by Fig. 6, where  $Q_{v,1}$  deals with the two incoming messages from CN (i.e.,  $(S_1, S_2)$ ), and  $Q_{v,2}$  deals with the incoming message  $(L, S')$  with  $L$  from channel and  $S'$  from the output of  $Q_{v,1}$ . The joint distribution  $P_{S_1,S_2|X}$  is given by Table II(a).  $Q_{v,1}$  is a quantizer maximizing  $I(X, S')$ , and we have

$$P_{S'|X}(s'|x) = \begin{cases} 8/9 & s' = 0, x = 0, \\ 1/9 & s' = 1, x = 0, \\ 5/9 & s' = 0, x = 1, \\ 4/9 & s' = 1, x = 1. \end{cases} \quad (14)$$

Using  $L$  and  $S'$  as input messages, the joint distribution  $P_{L,S'|X}$  is given by Table II(b).  $Q_{v,2}$  is an MIM quantizer (in the sense that  $(L, S')$  is the input message) maximizing  $I(X; R)$  with  $I(X; R) = 0.223$ . The  $Q_v$  corresponding to  $Q_{v,1}$  and  $Q_{v,2}$  of Table II can be written as

$$Q_v(l, s_1, s_2) = Q_{v,2}(l, Q_{v,1}(s_1, s_2)) = \begin{cases} 0 & (l, s_1, s_2) = (0, 0, 0), (0, 0, 1), (0, 1, 0), \\ 1 & \text{otherwise,} \end{cases} \quad (15)$$

TABLE II  
JOINT DISTRIBUTIONS AND OPTIMAL QUANTIZERS AFTER  
DECOMPOSITION

(a) Joint Distribution  $P_{S_1, S_2|X}$  and the Optimal Quantizer  $Q_{v,1}$ , where  $(s_1, s_2)$  Is Listed in Descending Order from Top to Bottom Based on  $P_{S_1, S_2|X}(\cdot|0)/P_{S_1, S_2|X}(\cdot|1)$

$(s_1, s_2)$	$P_{S_1, S_2 X}(\cdot 0)$	$P_{S_1, S_2 X}(\cdot 1)$	$Q_{v,1}(\cdot)$
(0, 0)	4/9	1/9	0
(0, 1)	2/9	2/9	0
(1, 0)	2/9	2/9	0
(1, 1)	1/9	4/9	1

(b) Joint Distribution  $P_{L, S'|X}$  and the Optimal Quantizer  $Q_{v,2}$ , where  $(l, s')$  Is Listed in Descending Order from Top to Bottom Based on  $P_{L, S'|X}(\cdot|0)/P_{L, S'|X}(\cdot|1)$

$(l, s')$	$P_{L, S' X}(\cdot 0)$	$P_{L, S' X}(\cdot 1)$	$Q_{v,2}(\cdot)$
(0, 0)	24/36	5/36	0
(0, 1)	3/36	4/36	1
(1, 0)	8/36	15/36	1
(1, 1)	1/36	12/36	1

which leads to a smaller  $I(X; R)$  (i.e., 0.223) than that associated with the  $Q_v$  (given by Table I) due to the decomposition.  $\square$

To overcome the drawback of the MIM-LUT decoding methods [7]–[14] due to the use of LUTs, in this work, we propose a systematic method, called MIM-QBP decoding, which is implemented based only on simple mappings and additions. Instead of using the decomposition technique, our method can deal with all incoming messages at a node (CN/VN) at the same time without causing any storage problem. The MIM-QBP decoding is presented in the next two subsections, for the updates at CN and VN, respectively.

### B. CN Update for MIM-QBP Decoding

The framework of CN update for MIM-QBP decoding is shown by Fig. 7. We implement the CN update with three steps: First, we use a function  $\phi_c$  to map each incoming message symbol to a number; second, we use a function  $\Phi_c$  to sum up all incoming messages' numbers (a little different from the summation in general meaning); third, we use an SDQ  $\Gamma_c$  to map the summation to the outgoing message symbol. In this way, the CN UF  $Q_c$  is fully determined by  $\phi_c, \Phi_c$ , and  $\Gamma_c$ . In the rest of this subsection, we show the principles for designing  $\phi_c, \Phi_c$ , and  $\Gamma_c$  so as to result in a  $Q_c$  which tends to maximize  $I(X; S)$ .

First, we use a reconstruction function (RF)

$$\phi_c : \mathcal{R} \rightarrow \mathbb{D} \quad (16)$$

to map each incoming message realization  $r \in \mathcal{R}$  to a specific number  $\phi_c(r)$  in the computational domain  $\mathbb{D}$ , where

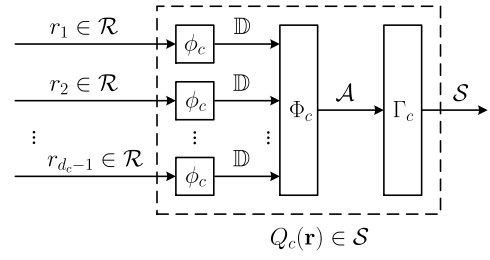


Fig. 7. Check node update for mutual information-maximizing quantized belief propagation (MIM-QBP) decoding. The part enclosed by the dash square corresponds to the update operation in the CN of Fig. 3(a).

in general  $\mathbb{D} = \mathbb{R}$  or  $\mathbb{D} = \mathbb{Z}$  is considered. Let  $\text{sgn}(\alpha)$  be the sign of  $\alpha \in \mathbb{R}$  given by

$$\text{sgn}(\alpha) = \begin{cases} -1 & \alpha < 0, \\ 0 & \alpha = 0, \\ 1 & \alpha > 0. \end{cases}$$

For  $r \in \mathcal{R}$ , let

$$LLR(r) = \log(P_{X|R}(0|r)/P_{X|R}(1|r)).$$

We suggest  $\phi_c(r)$  to satisfy

$$\begin{cases} \text{sgn}(\phi_c(r)) = \text{sgn}(LLR(r)), \\ |\phi_c(r)| \propto \frac{1}{|LLR(r)|}. \end{cases} \quad (17)$$

This suggestion associates  $\phi_c(r)$  to the channel input bit  $X$  in the following way: we predict  $X$  to be 0 if  $\text{sgn}(\phi_c(r)) > 0$  and to be 1 if  $\text{sgn}(\phi_c(r)) < 0$ , while  $|\phi_c(r)|$  indicates the *unreliability* of the prediction result.

Second, we represent each incoming message realization  $\mathbf{r} \in \mathcal{R}^{d_c-1}$  by

$$\Phi_c(\mathbf{r}) = \left( \prod_{i=1}^{\dim(\mathbf{r})} \text{sgn}(\phi_c(r_i)) \right) \sum_{i=1}^{\dim(\mathbf{r})} |\phi_c(r_i)|. \quad (18)$$

We predict  $X$  to be 0 if  $\text{sgn}(\Phi_c(\mathbf{r})) = \prod_{i=1}^{\dim(\mathbf{r})} \text{sgn}(\phi_c(r_i)) > 0$  and to be 1 if  $\text{sgn}(\Phi_c(\mathbf{r})) < 0$ , while  $|\Phi_c(\mathbf{r})| = \sum_{i=1}^{\dim(\mathbf{r})} |\phi_c(r_i)|$  indicates the *unreliability* of the prediction result. Prediction in this way is consistent with the true situation shown by Fig. 4:  $X$  is the binary summation of the channel input bits associated with  $\mathbf{r}$  (determined by  $\text{sgn}(\phi_c(r_i)), i = 1, 2, \dots, d_c - 1$ ), and more incoming messages lead to more unreliability (i.e., larger  $\dim(\mathbf{r})$  leads to larger  $|\Phi_c(\mathbf{r})|$ . This is the reason why we regard  $|\phi_c(r)|$  as the unreliability.). Denote

$$\mathcal{A} = \{a_1, a_2, \dots, a_{|\mathcal{A}|}\} = \{\Phi_c(\mathbf{r}) : \mathbf{r} \in \mathcal{R}^{d_c-1}\}. \quad (19)$$

Elements in  $\mathcal{A}$  are labelled to satisfy

$$a_1 \succ a_2 \succ \dots \succ a_{|\mathcal{A}|}, \quad (20)$$

where  $\succ$  is a binary relation on  $\mathbb{R}$  defined by

$$\alpha \succ \beta \iff \text{sgn}(\alpha) > \text{sgn}(\beta) \text{ or } (\text{sgn}(\alpha) = \text{sgn}(\beta) \text{ and } \alpha < \beta)$$

for  $\alpha, \beta \in \mathbb{R}$ . Assuming  $\Phi_c(\mathbf{r}) = a_i$ , from (20) we know that we are more likely to predict  $X$  to be 0 for smaller  $i$  and to be 1 for larger  $i$ . Let  $\mathcal{A}$  be a random variable taking values from  $\mathcal{A}$ . We have

$$P_{A|X}(a_i|x) = \sum_{\mathbf{r} \in \mathcal{R}^{d_c-1}, \Phi_c(\mathbf{r})=a_i} P_{\mathbf{R}|X}(\mathbf{r}|x), \quad (21)$$

where  $1 \leq i \leq |\mathcal{A}|$  and  $P_{\mathbf{R}|X}(\mathbf{r}|x)$  is given by (5).

Third, starting from  $\mathcal{A}$  and  $P_{A|X}$ , we can use the general DP method proposed in [16] to find an SDQ

$$\Lambda_c = \{\lambda_0 = 0, \lambda_1, \dots, \lambda_{|\mathcal{S}|-1}, \lambda_{|\mathcal{S}|} = |\mathcal{A}|\} : \mathcal{A} \rightarrow \mathcal{S} \quad (22)$$

to maximize  $I(X; S)$  (in the sense that the labelling of elements in  $\mathcal{A}$  is fixed and given by (20) and  $\Lambda_c$  is an SDQ). We also use  $\Lambda_c$  to generate the threshold set (TS)  $\Gamma_c$  given by

$$\Gamma_c = \{\gamma_i : 1 \leq i < |\mathcal{S}|, \gamma_i = a_{\lambda_i}\}. \quad (23)$$

Note that  $\Gamma_c$  is equivalent to  $\Lambda_c$  in quantizing  $\mathcal{A}$  to  $\mathcal{S}$ .

Finally, the UF  $Q_c : \mathcal{R}^{d_c-1} \rightarrow \mathcal{S}$  is fully determined by  $\phi_c, \Phi_c$ , and  $\Gamma_c$  in the following way given by

$$Q_c(\mathbf{r}) = \begin{cases} 0 & \Phi_c(\mathbf{r}) \succeq \gamma_1, \\ |\mathcal{S}| - 1 & \gamma_{|\mathcal{S}|-1} \succ \Phi_c(\mathbf{r}), \\ i & \gamma_i \succ \Phi_c(\mathbf{r}) \succeq \gamma_{i+1}, 1 \leq i \leq |\mathcal{S}| - 2, \end{cases} \quad (24)$$

where  $\succeq$  is a binary relation on  $\mathbb{R}$  defined by

$$\alpha \succeq \beta \iff \alpha \succ \beta \text{ or } \alpha = \beta$$

for  $\alpha, \beta \in \mathbb{R}$ . In addition, instead of using (7), we can compute  $P_{S|X}$  for the outgoing message  $S$  in a simpler way based on  $\Lambda_c$  given by

$$P_{S|X}(s|x) = \sum_{i=\lambda_s+1}^{\lambda_{s+1}} P_{A|X}(a_i|x). \quad (25)$$

Note that  $Q_c$  is essentially determined by  $\phi_c$ , since  $\Phi_c$  and  $\Gamma_c$  can be computed accordingly after  $\phi_c$  is given. We will illustrate the practical design of  $\phi_c$  in Section IV-A. After finishing the design of  $Q_c$  given by (24), the storage complexity for storing  $Q_c$  is  $O(|\mathcal{R}| + |\mathcal{S}|)$  ( $O(|\mathcal{R}|)$  for storing  $\phi_c$  and  $O(|\mathcal{S}|)$  for storing  $\Gamma_c$ ), and thus is negligible. On the other hand, implementing the CN update shown by Fig. 7 for computing *one* outgoing message has complexity  $O(d_c + \lceil \log_2(|\mathcal{S}|) \rceil)$ . In detail, computing  $\Phi_c(\mathbf{r})$  has complexity  $O(d_c)$  (binary operations mainly including additions), which allows a binary tree-like parallel implementation; meanwhile, mapping  $\Phi_c(\mathbf{r})$  to  $S$  based on  $\Gamma_c$  has complexity  $O(\lceil \log_2(|\mathcal{S}|) \rceil)$  (binary comparison operations), which can be analogously explained by Fig. 2. The fast and simple implementation for mapping  $\Phi_c(\mathbf{r})$  to  $S$  indeed benefits from the use of SDQs in (22) and (23). This is the essential reason why we choose SDQs. Instead, if an optimal DQ is used to map  $\mathcal{A}$  to  $\mathcal{S}$  in (22), we may in general need a table of size  $|\mathcal{A}|$  to store this optimal DQ, but at the same time, we may achieve better  $I(X; S)$  and can reduce the computational complexity for mapping  $\Phi_c(\mathbf{r})$  to  $S$  from  $O(\lceil \log_2(|\mathcal{S}|) \rceil)$  to  $O(1)$ .

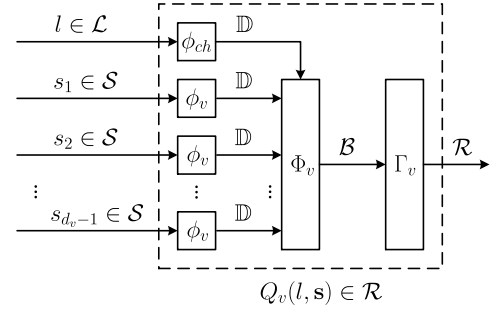


Fig. 8. Variable node update for mutual information-maximizing quantized belief propagation (MIM-QBP) decoding. The part enclosed by the dash square corresponds to the update operation in the VN of Fig. 3(b).

### C. VN Update for MIM-QBP Decoding

The framework of VN update for MIM-QBP decoding is shown by Fig. 8. We implement the VN update with three steps: First, we use two functions  $\phi_v$  and  $\phi_{ch}$  to map each incoming message symbol from CN and channel, respectively, to a number; second, we use a function  $\Phi_v$  to sum up all incoming messages' numbers; third, we use an SDQ  $\Gamma_v$  to map the summation to the outgoing message symbol. In this way, the VN UF  $Q_v$  is fully determined by  $\phi_v, \phi_{ch}, \Phi_v$ , and  $\Gamma_v$ . In the rest of this subsection, we show the principles for designing  $\phi_v, \phi_{ch}, \Phi_v$ , and  $\Gamma_v$  so as to result in a  $Q_v$  which tends to maximize  $I(X; R)$ .

First, we use a RF

$$\phi_v : \mathcal{S} \rightarrow \mathbb{D} \quad (26)$$

to map each incoming message (from CN) realization  $s \in \mathcal{S}$  to  $\phi_v(s) \in \mathbb{D}$ , and use another RF

$$\phi_{ch} : \mathcal{L} \rightarrow \mathbb{D} \quad (27)$$

to map the incoming message (from channel) realization  $l \in \mathcal{L}$  to  $\phi_{ch}(l) \in \mathbb{D}$ . For  $s \in \mathcal{S}$ , let

$$LLR(s) = \log(P_{X|S}(0|s)/P_{X|S}(1|s)).$$

For  $l \in \mathcal{L}$ , let

$$LLR(l) = \log(P_{X|L}(0|l)/P_{X|L}(1|l)).$$

We suggest  $\phi_v(s)$  and  $\phi_{ch}(l)$  to satisfy

$$\begin{cases} \phi_v(s) \propto LLR(s), \\ \phi_{ch}(l) \propto LLR(l). \end{cases} \quad (28)$$

This suggestion associates  $\phi_v(s)$  and  $\phi_{ch}(l)$  to the channel input bit  $X$  in the following way:  $X$  is more likely to be 0 (resp. 1) for larger (resp. smaller)  $\phi_v(s)$  and  $\phi_{ch}(l)$ .

Second, we represent each incoming message realization  $(l, s) \in \mathcal{L} \times \mathcal{S}^{d_v-1}$  by

$$\Phi_v(l, \mathbf{s}) = \phi_{ch}(l) + \sum_{i=1}^{\dim(\mathbf{s})} \phi_v(s_i). \quad (29)$$

The channel input bit  $X$  is more likely to be 0 (resp. 1) for larger (resp. smaller)  $\Phi_v(l, s)$ . Denote

$$\mathcal{B} = \{b_1, b_2, \dots, b_{|\mathcal{B}|}\} = \{\Phi_v(l, s) : (l, s) \in \mathcal{L} \times \mathcal{S}^{d_v-1}\}. \quad (30)$$

Elements in  $\mathcal{B}$  are labelled to satisfy

$$b_1 > b_2 > \dots > b_{|\mathcal{B}|}. \quad (31)$$

Assuming  $\Phi_v(l, s) = b_i$ , from (31) we know that  $X$  is more likely to be 0 (resp. 1) for larger (resp. smaller)  $i$ . Let  $B$  be a random variable taking values from  $\mathcal{B}$ . We have

$$P_{B|X}(b_i|x) = \sum_{(l,s) \in \mathcal{L} \times \mathcal{S}^{d_v-1}, \Phi_v(l,s)=b_i} P_{L,S|X}(l,s|x), \quad (32)$$

where  $1 \leq i \leq |\mathcal{B}|$  and  $P_{L,S|X}(l,s|x)$  is given by (9).

Third, starting from  $\mathcal{B}$  and  $P_{B|X}$ , we can use the general DP method proposed in [16] to find an SDQ

$$\Lambda_v = \{\lambda_0 = 0, \lambda_1, \dots, \lambda_{|\mathcal{R}|-1}, \lambda_{|\mathcal{R}|} = |\mathcal{B}|\} : \mathcal{B} \rightarrow \mathcal{R} \quad (33)$$

to maximize  $I(X; R)$  (in the sense that the labelling of elements in  $\mathcal{B}$  is fixed and given by (31) and  $\Lambda_v$  is an SDQ). We also use  $\Lambda_v$  to generate the TS given by

$$\Gamma_v = \{\gamma_i : 1 \leq i < |\mathcal{R}|, \gamma_i = b_{\lambda_i}\}. \quad (34)$$

Note that  $\Gamma_v$  is equivalent to  $\Lambda_v$  in quantizing  $\mathcal{B}$  to  $\mathcal{R}$ .

Finally, the UF  $Q_v : \mathcal{L} \times \mathcal{S}^{d_v-1} \rightarrow \mathcal{R}$  is fully determined by  $\phi_v, \phi_{ch}, \Phi_v$ , and  $\Gamma_v$  in the following way given by

$$Q_v(l, s) = \begin{cases} 0 & \Phi_v(l, s) \geq \gamma_1, \\ |\mathcal{R}| - 1 & \Phi_v(l, s) < \gamma_{|\mathcal{R}|-1}, \\ i & \gamma_i > \Phi_v(l, s) \geq \gamma_{i+1}, 1 \leq i \leq |\mathcal{R}| - 2. \end{cases} \quad (35)$$

In addition, instead of using (10), we can compute  $P_{R|X}$  for the outgoing message  $R$  in a simpler way based on  $\Lambda_v$  given by

$$P_{R|X}(r|x) = \sum_{i=\lambda_r+1}^{\lambda_{r+1}} P_{B|X}(b_i|x). \quad (36)$$

Note that  $Q_v$  is essentially determined by  $\phi_v$  and  $\phi_{ch}$ , since  $\Phi_v$  and  $\Gamma_v$  can be computed accordingly after  $\phi_v$  and  $\phi_{ch}$  are given. We will illustrate the practical design of  $\phi_v$  and  $\phi_{ch}$  in Section IV-B. After finishing the design of  $Q_v$  given by (35), the storage complexity for storing  $Q_v$  is  $O(|\mathcal{S}| + |\mathcal{L}| + |\mathcal{R}|)$  ( $O(|\mathcal{S}|)$  for storing  $\phi_v$ ,  $O(|\mathcal{L}|)$  for storing  $\phi_{ch}$ , and  $O(|\mathcal{R}|)$  for storing  $\Gamma_v$ ), and thus is negligible. On the other hand, implementing the VN update shown by Fig. 8 for computing *one* outgoing message has complexity  $O(d_v + \lceil \log_2(|\mathcal{R}|) \rceil)$ . In detail, computing  $\Phi_v(l, s)$  has complexity  $O(d_v)$ , which allows a binary tree-like parallel implementation; meanwhile, mapping  $\Phi_v(l, s)$  to  $R$  based on  $\Gamma_v$  has complexity  $O(\lceil \log_2(|\mathcal{R}|) \rceil)$ , which can be analogously explained by Fig. 2. The fast and simple implementation for mapping  $\Phi_c(l, s)$  to  $R$  also benefits from the use of SDQs in (33) and (34). If we use the optimal DQ instead, we may in general need a table of size  $|\mathcal{B}|$  to store this optimal DQ, but at the same time, we may achieve better  $I(X; R)$  and can

reduce the computational complexity for mapping  $\Phi_c(l, s)$  to  $R$  from  $O(\lceil \log_2(|\mathcal{R}|) \rceil)$  to  $O(1)$ .

*Example 2:* We show a practical case for the framework in Fig. 8 to apply. Consider Example 1 again. If we use  $\phi_v$  with

$$\phi_v(s) = \begin{cases} 1 & s = 0, \\ 0 & s = 1, \end{cases}$$

and use  $\phi_{ch}$  with

$$\phi_{ch}(l) = \begin{cases} 1 & l = 0, \\ 0 & l = 1, \end{cases}$$

the TS  $\Gamma_v$  defined by (34) will be given by

$$\Gamma_v = \{\gamma_1 = 2\}.$$

Then,  $Q_v$  defined by (35) will be totally the same with the  $Q_v$  defined by Table I, which maximizes  $I(X, R)$  with  $I(X, R) = 0.236$ . Therefore, instead of using Table I to store  $Q_v$ , we can use  $\phi_v, \phi_{ch}, \Phi_v$ , and  $\Gamma_v$  to fully determine  $Q_v$  in the way of (35).

#### D. Remarks

For each decoding iteration, the design of  $Q_e : \mathcal{L} \times \mathcal{S}^{d_v} \rightarrow \mathcal{X}$  for the MIM-QBP decoding is quite similar to the design of  $Q_v$  introduced in Section III-C. In particular, the same RFs  $\phi_v$  and  $\phi_{ch}$  can be used for the design of  $Q_e$  and  $Q_v$  for a same decoding iteration. We thus ignore the details.

The MIM-QBP decoding leads to a very practical decoder, namely the MIM-QBP decoder, which can be implemented based only on the RFs (i.e.,  $\phi_c, \phi_v$ , and  $\phi_{ch}$ ), the TSs (i.e.,  $\Gamma_c$  and  $\Gamma_v$ , derived from the RFs off-line), and the additions (i.e.,  $\Phi_c$  and  $\Phi_v$ ). Compared to the MIM-LUT decoder, the MIM-QBP decoder can greatly save memory costs. Given the design noise standard deviation  $\sigma_d$  (i.e., given  $P_{L|X}$ ), the design of the MIM-QBP decoder is essentially determined by the design of the RFs  $\phi_c, \phi_v$ , and  $\phi_{ch}$ , which is indeed an off-line task. We will deal with this task in the next section.

#### IV. PRACTICAL DESIGN OF MIM-QBP DECODER

The MIM-QBP decoder proposed in Section III works similarly to those presented by [4]–[6]. In fact, we borrow the terms “reconstruction function”, “computational domain”, “unreliability”, and “threshold set” from [4]–[6]. However, unlike the authors of [4]–[6] used hand optimization to design their decoders, we show how to practically and systematical design the MIM-QBP decoder in this section.

As discussed in Section III, given the design noise standard deviation  $\sigma_d$ , the design of the MIM-QBP decoder is essentially determined by the design of the RFs  $\phi_c, \phi_v$ , and  $\phi_{ch}$ . One possible solution to this design problem is to use some search methods, like the differential evolution [19], to search for good RFs based on the suggestions of (17) and (28) so as to maximize  $I(X; S)$  and  $I(X; R)$ . Instead, our solution is to first give the close form of the optimal RFs, say  $\phi_c^*, \phi_v^*$ , and  $\phi_{ch}^*$ , which can maximize  $I(X; S)$  and  $I(X; R)$ . Then, since the optimal RFs work in the real domain (i.e.,  $\mathbb{D} = \mathbb{R}$ ), we design the RFs by properly scaling the optimal RFs to an integer range of interest for practical purpose.

### A. MIM-QBP Decoder Design at CN

Let  $g(r) = P_{X|R}(0|r) - P_{X|R}(1|r)$  for  $r \in \mathcal{R}$  and  $g(\mathbf{r}) = P_{X|\mathbf{R}}(0|\mathbf{r}) - P_{X|\mathbf{R}}(1|\mathbf{r})$  for  $\mathbf{r} \in \mathcal{R}^{d_c-1}$ . For  $r \in \mathcal{R}$ , let

$$\phi_c^*(r) = \begin{cases} \text{sgn}(g(r))\epsilon & |g(r)| = 1, \\ -\text{sgn}(g(r))\log(|g(r)|) & \text{otherwise,} \end{cases} \quad (37)$$

where  $\epsilon$  satisfies

$$0 < \epsilon d_c < \min \{ |\log(|g(\mathbf{r})|) - \log(|g(\mathbf{r}')|)| : \mathbf{r}, \mathbf{r}' \in \mathcal{R}^{d_c-1}, g(\mathbf{r}) \neq g(\mathbf{r}'), \text{sgn}(g(\mathbf{r})) = \text{sgn}(g(\mathbf{r}')) \neq 0 \}. \quad (38)$$

We use  $\epsilon$  to ensure the condition of (17) for  $\phi_c = \phi_c^*$ .

**Theorem 1:** If  $\phi_c = \phi_c^*$ ,  $Q_c$  defined by (24) can maximize  $I(X; S)$  among all the functions mapping  $\mathcal{R}^{d_c-1}$  to  $\mathcal{S}$ .

*Proof:* See Appendix A. ■

Theorem 1 indicates that  $\phi_c^*$  is an optimal choice for  $\phi_c$  in terms of maximizing  $I(X; S)$ . Note that the function  $f(x) = \log((e^x + 1)/(e^x - 1))$ , which was used in [1] for implementing the CN update for BP decoding, is closely related to  $\phi_c^*$  in terms of  $f(|LLR(r)|) = -\log(|g(r)|)$  and  $\text{sgn}(LLR(r)) = \text{sgn}(g(r))$  for  $r \in \mathcal{R}$ . In addition, we deal with all incoming messages by  $\Phi_c$ , which indeed works similarly to the way based on  $f(x)$  in [1]. This simple discussion implies a close relation between the CN updates of the BP decoding and the MIM-QBP decoding for the case  $\phi_c = \phi_c^*$ .

$\phi_c^*$  requires the computational domain  $\mathbb{D}$  to be  $\mathbb{R}$ , while  $\mathbb{D} = \mathbb{Z}$  is more suitable for a practical situation for simple hardware implementation. In the following, we design  $\phi_c : \mathcal{R} \rightarrow \mathbb{Z}$  based on  $\phi_c^*$  for practical purpose.

**Corollary 1:** Let  $\eta$  be a positive number. If  $\phi_c = \eta\phi_c^*$ ,  $Q_c$  defined by (24) can maximize  $I(X; S)$  among all the functions mapping  $\mathcal{R}^{d_c-1}$  to  $\mathcal{S}$ .

*Proof:* Corollary 1 can be proved in a way similarly to prove Theorem 1. ■

Denote the maximum allowed absolute value of  $\phi_c(\cdot)$  by  $|\phi_c|_{\max}$ . Let

$$|\phi_c^*|_{\max} = \max\{|\phi_c^*(r)| : r \in \mathcal{R}, g(r) \neq 0\}.$$

Note that  $|\phi_c^*|_{\max} > 0$  holds for a general practical case. Then, inspired by Corollary 1, we design  $\phi_c : \mathcal{R} \rightarrow \mathbb{Z}$  by scaling  $\phi_c^*$  (loosely speaking, by factors around  $\eta = |\phi_c|_{\max}/|\phi_c^*|_{\max}$ ) to the valid integer range  $[-|\phi_c|_{\max}, |\phi_c|_{\max}]$  in the way below

$$\phi_c(r) = \begin{cases} \text{sgn}(g(r)) \max\{1, \lfloor |\phi_c^*(r)| \cdot |\phi_c|_{\max}/|\phi_c^*|_{\max} + 0.5 \rfloor\} & g(r) \neq 0, \\ |\phi_c|_{\max} & g(r) = 0, \end{cases} \quad (39)$$

where for  $g(r) \neq 0$ , we make  $\phi_c(r) \neq 0$  to ensure  $\text{sgn}(\phi_c(r)) = \text{sgn}(g(r))$ . Meanwhile, for  $g(r) = 0$ , we use  $\phi_c(r) = |\phi_c|_{\max}$  instead of  $\phi_c(r) = 0$  because the existing of  $\phi_c(r) = 0$  will bring two disadvantages: i) two bits are needed for representing the sign of  $\phi_c$ , and ii) it is not applicable for computing the sign of the  $j$ -th outgoing message during decoding in the way of  $(\prod_{i=1}^{d_c} \text{sgn}(\phi_c(r_i)))/\text{sgn}(\phi_c(r_j))$

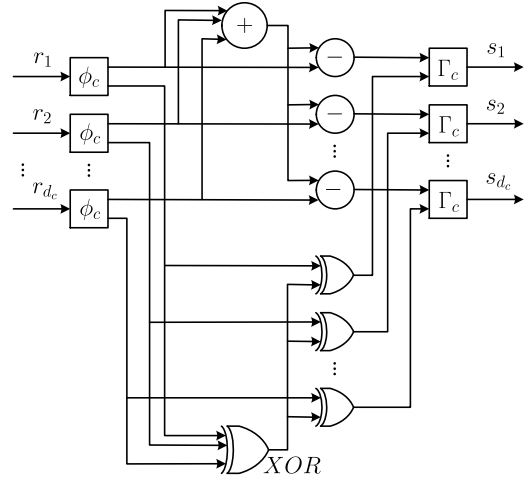


Fig. 9. Hardware architecture (similar to that given by [5, Fig. 2]) for the check node update of mutual information-maximizing quantized belief propagation (MIM-QBP) decoder. The adders/subtractors and XOR gates are used for computing  $\sum_{i=1}^{d_c} |\phi_c(r_i)| - |\phi_c(r_j)|$  and  $(\prod_{i=1}^{d_c} \text{sgn}(\phi_c(r_i)))/\text{sgn}(\phi_c(r_j))$ , respectively, for  $j = 1, 2, \dots, d_c$ . This architecture is applicable when  $\text{sgn}(\phi_c(\cdot)) \in \{1, -1\}$ .

for  $j = 1, 2, \dots, d_c$ , which way has a simple hardware-implementing architecture as shown by Fig. 9. Moreover, according to our simulations, the situation where  $g(r) = 0$  hardly occurs; meanwhile,  $\phi_c(r) = |\phi_c|_{\max}$  and  $\phi_c(r) = 0$  do not make non-negligible difference in terms of error performance.

Suppose the decoder is allowed to use at most  $q_c$  bits for the additions for computing each outgoing message (refer to  $\Phi_c$  defined by (18)). Note that one bit is needed for computing the sign of each outgoing message. Then,  $|\phi_c|_{\max}$  is given by

$$|\phi_c|_{\max} = \lfloor (2^{q_c-1} - 1)/d_c \rfloor \quad (40)$$

such that  $\sum_{i=1}^{d_c} |\phi_c(r_i)|$  does not overflow and the decoder can use the simple architecture given by Fig. 9 to compute each outgoing message.

After the design of RFs given by (39),  $\Phi_c$  defined by (18) is a function mapping  $\mathcal{R}^{d_c-1}$  to  $\mathbb{Z}$  and the resulting integers can be represented by  $q_c$  bits. Moreover, we can compute  $\mathcal{A}$  and  $P_{A|X}$  in a much faster way than using (19) and (21), respectively, while the computation in the ways of (19) and (21) can be a prohibitive task when  $|\mathcal{R}|^{d_c-1}$  is large. In the following, we propose a fast method to compute  $\mathcal{A}$  and  $P_{A|X}$ .

**Theorem 2:** For  $k \geq 1$  and  $\mathbf{R} \in \mathcal{R}^k$ , let

$$P_{\mathbf{R}|X}(\mathbf{r}|x) = \left(\frac{1}{2}\right)^{\dim(\mathbf{r})-1} \sum_{\mathbf{x}: \oplus \mathbf{x} = x} \prod_{i=1}^{\dim(\mathbf{r})} P_{R_i|X}(r_i|x_i).$$

In addition, let

$$\mathcal{A}_k = \{a_{k,1}, a_{k,2}, \dots, a_{k,|\mathcal{A}_k|}\} = \{\Phi_c(\mathbf{r}) : \mathbf{r} \in \mathcal{R}^k\}$$

and  $A_k$  be a random variable taking values from  $\mathcal{A}_k$ . Moreover, define  $\delta_k^+(\cdot)$  and  $\delta_k^-(\cdot)$  by

$$\delta_k^\pm(a_{k,i}) = P_{A_k|X}(a_{k,i}|0) \pm P_{A_k|X}(a_{k,i}|1).$$



Then, for  $k = 1$ , we have

$$\mathcal{A}_k = \{\phi_c(r) : r \in \mathcal{R}\},$$

$$\delta_k^\pm(a_{k,i}) = \sum_{r \in \mathcal{R}, \phi_c(r)=a_{k,i}} (P_{R|X}(r|0) \pm P_{R|X}(r|1)). \quad (41)$$

For  $k > 1$ , we have

$$\mathcal{A}_k = \{\phi_c(r) \diamond a_{k-1,j} : r \in \mathcal{R}, a_{k-1,j} \in \mathcal{A}_{k-1}\},$$

$$\delta_k^\pm(a_{k,i}) = \sum_{\substack{r \in \mathcal{R}, a_{k-1,j} \in \mathcal{A}_{k-1}, \\ \phi_c(r) \diamond a_{k-1,j} = a_{k,i}}} \frac{1}{2} (P_{R|X}(r|0) \pm P_{R|X}(r|1)) \delta_{k-1}^\pm(a_{k-1,j}), \quad (42)$$

where  $\diamond$  is a binary operator given by

$$\alpha \diamond \beta = \text{sgn}(\alpha) \text{sgn}(\beta) (|\alpha| + |\beta|)$$

for  $\alpha, \beta \in \mathbb{R}$ .

*Proof:* For  $k = 1$ , (41) holds obviously. For  $k > 1$ , we have

$$\begin{aligned} \mathcal{A}_k &= \{\Phi_c(\mathbf{r}) : \mathbf{r} \in \mathcal{R}^k\} \\ &= \{\phi_c(r) \diamond \Phi_c(\mathbf{r}) : r \in \mathcal{R}, \mathbf{r} \in \mathcal{R}^{k-1}\} \\ &= \{\phi_c(r) \diamond a_{k-1,j} : r \in \mathcal{R}, a_{k-1,j} \in \mathcal{A}_{k-1}\}; \end{aligned}$$

meanwhile, we have

$$\begin{aligned} \delta_k^\pm(a_{k,i}) &= \sum_{\mathbf{r} \in \mathcal{R}^k, \Phi_c(\mathbf{r})=a_{k,i}} (P_{\mathbf{R}|\mathbf{X}}(\mathbf{r}|0) \pm P_{\mathbf{R}|\mathbf{X}}(\mathbf{r}|1)) \\ &= \sum_{\mathbf{r} \in \mathcal{R}^k, \Phi_c(\mathbf{r})=a_{k,i}} \left(\frac{1}{2}\right)^{k-1} \prod_{u=1}^k (P_{R|X}(r_u|0) \pm P_{R|X}(r_u|1)) \\ &= \sum_{r_k \in \mathcal{R}} \frac{1}{2} (P_{R|X}(r_k|0) \pm P_{R|X}(r_k|1)) \cdot \\ &\quad \sum_{\substack{\mathbf{r} \in \mathcal{R}^{k-1}, \\ \phi_c(r) \diamond \Phi_c(\mathbf{r})=a_{k,i}}} \left(\frac{1}{2}\right)^{k-2} \prod_{u=1}^{k-1} (P_{R|X}(r_u|0) \pm P_{R|X}(r_u|1)) \\ &= \sum_{r_k \in \mathcal{R}} \frac{1}{2} (P_{R|X}(r_k|0) \pm P_{R|X}(r_k|1)) \cdot \\ &\quad \sum_{\substack{\mathbf{r} \in \mathcal{R}^{k-1}, \\ \phi_c(r) \diamond \Phi_c(\mathbf{r})=a_{k,i}}} (P_{\mathbf{R}|\mathbf{X}}(\mathbf{r}|0) \pm P_{\mathbf{R}|\mathbf{X}}(\mathbf{r}|1)) \\ &= \sum_{r \in \mathcal{R}} \frac{1}{2} (P_{R|X}(r|0) \pm P_{R|X}(r|1)) \sum_{\substack{a_{k-1,j} \in \mathcal{A}_{k-1}, \\ \phi_c(r) \diamond a_{k-1,j} = a_{k,i}}} \delta_{k-1}^\pm(a_{k-1,j}). \end{aligned}$$

This completes the proof.  $\blacksquare$

According to Theorem 2, we can compute  $\mathcal{A}_1, \delta_1^\pm, \mathcal{A}_2, \delta_2^\pm, \dots, \mathcal{A}_{d_c-1}, \delta_{d_c-1}^\pm$  sequentially. Then,  $\mathcal{A}$  and  $P_{A|X}$  equal to  $\mathcal{A}_{d_c-1}$  and  $P_{\mathcal{A}_{d_c-1}|X}$ , respectively, where  $P_{\mathcal{A}_{d_c-1}|X}$  can be easily computed based on  $\delta_{d_c-1}^\pm$ . We summarize the computation by Algorithm 1. Since  $|\mathcal{A}_{k-1}|$  in line 7 of Algorithm 1 is upper-bounded by  $2^{q_c}$ , the complexity of Algorithm 1 is  $O(d_c 2^{q_c} |\mathcal{R}|)$ .

---

**Algorithm 1** Computation of  $\mathcal{A}$  and  $P_{A|X}$

---

**Input:**  $P_{R|X}, \phi_c, d_c$ .

**Output:**  $\mathcal{A}$  and  $P_{A|X}$ .

---

```

1: Set  $\mathcal{A}_k = \emptyset$  and  $\delta_k^\pm(\cdot) = 0$  for  $k = 1, 2, \dots, d_c - 1$ .
2: for  $r \in \mathcal{R}$  do
3:    $\mathcal{A}_1 = \mathcal{A}_1 \cup \{\phi_c(r)\}$ . //See (41)
4:    $\delta_1^\pm(\phi_c(r)) = P_{R|X}(r|0) \pm P_{R|X}(r|1)$ .
5: end for
6: for  $k = 2, 3, \dots, d_c - 1$  do
7:   for  $r \in \mathcal{R}, a_{k-1,j} \in \mathcal{A}_{k-1}$  do
8:      $a_{k,i} = \phi_c(r) \diamond a_{k-1,j}$ .
9:      $\mathcal{A}_k = \mathcal{A}_k \cup \{a_{k,i}\}$ . //See (42)
10:     $\delta_k^\pm(a_{k,i}) = \frac{1}{2} (P_{R|X}(r|0) \pm P_{R|X}(r|1)) \delta_{k-1}^\pm(a_{k-1,j})$ .
11:   end for
12: end for
13: for  $k = 1, 2, \dots, d_c - 1$  do
14:   for  $a_{k,i} \in \mathcal{A}_k$  do
15:      $P_{\mathcal{A}_k|X}(a_{k,i}|0) = (\delta_k^+(a_{k,i}) + \delta_k^-(a_{k,i}))/2$ .
16:      $P_{\mathcal{A}_k|X}(a_{k,i}|1) = (\delta_k^+(a_{k,i}) - \delta_k^-(a_{k,i}))/2$ .
17:   end for
18: end for
19:  $\mathcal{A} = \mathcal{A}_{d_c-1}$ .
20:  $P_{A|X} = P_{\mathcal{A}_{d_c-1}|X}$ .
21: return  $\mathcal{A}$  and  $P_{A|X}$ .
```

---

At this point, starting from  $\mathcal{A}$  and  $P_{A|X}$ , we can compute the optimal SDQ  $\Lambda_c$  given by (22). The computational complexity is upper-bounded by  $O(2^{2q_c} |\mathcal{S}|)$  [15], [16]. For the special situation where  $P_{A|X}$  satisfies

$$\frac{P_{A|X}(a_1|0)}{P_{A|X}(a_1|1)} \geq \frac{P_{A|X}(a_2|0)}{P_{A|X}(a_2|1)} \geq \dots \geq \frac{P_{A|X}(a_{|\mathcal{A}|}|0)}{P_{A|X}(a_{|\mathcal{A}|}|1)}, \quad (43)$$

the computational complexity can be reduced to  $O(2^{q_c} |\mathcal{S}|)$  [16], [20]. The simulation results show that (43) frequently holds. This phenomenon is reasonable because  $\phi_c = \phi_c^*$  can always make (43) hold according to (53), while we set  $\phi_c$  by scaling  $\phi_c^*$  (see (39)). After the computation of  $\Lambda_c$ , we can then compute the TS  $\Gamma_c$ , the UF  $Q_c$ , and the pmf  $P_{S|X}$  given by (23), (24), and (25) respectively. Till now, the MIM-QBP decoder design at CN is completed, which has a total complexity upper-bounded by  $O(d_c 2^{q_c} |\mathcal{R}| + 2^{2q_c} |\mathcal{S}|)$  (for one decoding iteration).

After the design of the MIM-QBP decoder at CN, we can use the hardware architecture shown by Fig. 9 to implement the update at CN for computing all outgoing messages  $s_1, s_2, \dots, s_{d_c}$ . The computational complexity is  $O(d_c + d_c \lceil \log_2(|\mathcal{S}|) \rceil)$  for one CN for one iteration, where  $O(d_c)$  refers to the complexity of addition and XOR operations, and  $O(d_c \lceil \log_2(|\mathcal{S}|) \rceil)$  refers to the complexity of mapping operations based on  $\Gamma_c$  for the  $d_c$  outgoing messages.

### B. MIM-QBP Decoder Design at VN

For  $s \in \mathcal{S}$  and  $l \in \mathcal{L}$ , let

$$\begin{cases} \phi_v^*(s) = \log(P_{S|X}(s|0)/P_{S|X}(s|1)), \\ \phi_{ch}^*(l) = \log(P_{L|X}(l|0)/P_{L|X}(l|1)). \end{cases} \quad (44)$$

We can easily verify the condition of (28) holds for  $\phi_v = \phi_v^*$  and  $\phi_{ch} = \phi_{ch}^*$ .

**Theorem 3:** If  $\phi_v = \phi_v^*$  and  $\phi_{ch} = \phi_{ch}^*$ ,  $Q_v$  defined by (35) can maximize  $I(X; R)$  among all the functions mapping  $\mathcal{L} \times \mathcal{S}^{d_v-1}$  to  $\mathcal{R}$ .

*Proof:* See Appendix B. ■

Theorem 3 indicates that  $(\phi_v^*, \phi_{ch}^*)$  is an optimal choice for  $(\phi_c, \phi_{ch})$  in terms of maximizing  $I(X; R)$ . Note that  $\phi_v^*(s) = LLR(s) + \log(P_X(1)/P_X(0))$  and  $\phi_{ch}^*(l) = LLR(l) + \log(P_X(1)/P_X(0))$ , implying a close relation between the VN updates of the BP decoding and the MIM-QBP decoding for the case  $\phi_v = \phi_v^*$  and  $\phi_{ch} = \phi_{ch}^*$ . In the following, we design  $\phi_v : \mathcal{S} \rightarrow \mathbb{Z}$  and  $\phi_{ch} : \mathcal{L} \rightarrow \mathbb{Z}$  based on  $\phi_v^*$  and  $\phi_{ch}^*$  for practical purpose.

**Corollary 2:** Let  $\eta$  be a positive number. If  $\phi_v = \eta\phi_v^*$  and  $\phi_{ch} = \eta\phi_{ch}^*$ ,  $Q_v$  defined by (35) can maximize  $I(X; R)$  among all the functions mapping  $\mathcal{L} \times \mathcal{S}^{d_v-1}$  to  $\mathcal{R}$ .

*Proof:* Corollary 2 can be proved in a way similarly to prove Theorem 3. ■

Denote the maximum allowed absolute value of  $\phi_v(\cdot)$  and  $\phi_{ch}(\cdot)$  by  $|\phi_{v,ch}|_{max}$ . Let

$$|\phi_{v,ch}^*|_{max} = \max(\{|\phi_v^*(s)| : s \in \mathcal{S}\} \cup \{|\phi_{ch}^*(l)| : l \in \mathcal{L}\}).$$

Note that  $|\phi_{v,ch}^*|_{max} > 0$  holds for a general practical case. Then, inspired by Corollary 2, we design  $\phi_v : \mathcal{S} \rightarrow \mathbb{Z}$  and  $\phi_{ch} : \mathcal{L} \rightarrow \mathbb{Z}$  by scaling  $\phi_v^*$  and  $\phi_{ch}^*$  (loosely speaking, by factors around  $\eta = |\phi_{v,ch}|_{max}/|\phi_{v,ch}^*|_{max}$ ) to the valid integer range  $[-|\phi_{v,ch}|_{max}, |\phi_{v,ch}|_{max}]$  in the way below

$$\begin{cases} \phi_v(s) = \text{sgn}(\phi_v^*(s)) \cdot \lfloor |\phi_v^*(s)| \cdot |\phi_{v,ch}|_{max}/|\phi_{v,ch}^*|_{max} + 0.5 \rfloor, \\ \phi_{ch}(l) = \text{sgn}(\phi_{ch}^*(l)) \cdot \lfloor |\phi_{ch}^*(l)| \cdot |\phi_{v,ch}|_{max}/|\phi_{v,ch}^*|_{max} + 0.5 \rfloor. \end{cases} \quad (45)$$

Suppose the decoder is allowed to use at most  $q_v$  bits for the additions for computing each outgoing message (refer to  $\Phi_v$  defined by (29)). Then,  $|\phi_{v,ch}|_{max}$  used in our simulations is given by

$$|\phi_{v,ch}|_{max} = \lfloor (2^{q_v-1} - 1)/(d_v + 1) \rfloor. \quad (46)$$

Let  $|\phi_v|_{max} = \{|\phi_v(s)| : s \in \mathcal{S}\}$  and  $|\phi_{ch}|_{max} = \{|\phi_{ch}(l)| : l \in \mathcal{L}\}$ . (45) and (46) ensure that

$$|\phi_{ch}|_{max} + d_v |\phi_v|_{max} \leq 2^{q_v-1} - 1, \quad (47)$$

implying that the additions do not overflow. In this case, the decoder can compute the  $j$ -th outgoing message during decoding in the way of  $\phi_{ch}(l) + \sum_{i=1}^{d_v} \phi_v(r_i) - \phi_v(r_j)$  for  $j = 1, 2, \dots, d_v$ , which way can be implemented by using the simple hardware architecture given by Fig. 10. However, the gap  $(2^{q_v-1} - 1) - (|\phi_{ch}|_{max} + d_v |\phi_v|_{max})$  can be quite large especially for initial decoding iterations. For the purpose of

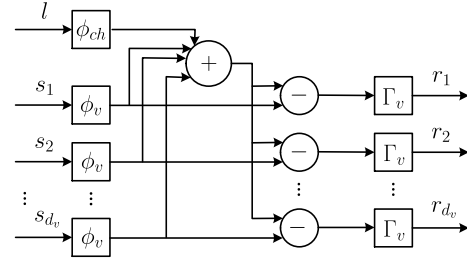


Fig. 10. Hardware architecture (similar to that given by [5, Fig. 3]) for the variable node update of mutual information-maximizing quantized belief propagation (MIM-QBP) decoder. The adders/subtractors are used for computing  $\phi_{ch}(l) + \sum_{i=1}^{d_v} |\phi_v(s_i)| - |\phi_v(s_j)|$  for  $j = 1, 2, \dots, d_v$ .

saving resource, we can use less than  $q_v$  bits for the additions without changing the RFs. Or instead, for the purpose of making full use of the  $q_v$  bits, we can find the largest  $|\phi_{v,ch}|_{max}$  to make  $|\phi_{ch}|_{max} + d_v |\phi_v|_{max}$  as close as possible to  $2^{q_v-1} - 1$  while maintaining (47), where this task can be efficiently done by applying binary search on  $|\phi_{v,ch}|_{max}$ .

After the design of RFs given by (45),  $\Phi_v$  defined by (29) is a function mapping  $\mathcal{L} \times \mathcal{S}^{d_v-1}$  to  $\mathbb{Z}$  and the resulting integers can be represented by  $q_v$  bits. Moreover, we can compute  $\mathcal{B}$  and  $P_{B|X}$  in a much faster way than using (30) and (32), respectively. Just like proposing Algorithm 1 for computing  $\mathcal{A}$  and  $P_{A|X}$ , we propose another fast method to compute  $\mathcal{B}$  and  $P_{B|X}$ .

**Theorem 4:** For  $k \geq 0, L \in \mathcal{L}$ , and  $\mathbf{S} \in \mathcal{S}^k$ , let

$$P_{L,\mathbf{S}|X}(l, \mathbf{s}|x) = P_{L|X}(l|x) \prod_{i=1}^{\dim(\mathbf{s})} P_{S|X}(s_i|x),$$

where for  $k = 0$ , let

$$P_{L,\mathbf{S}|X}(l, \mathbf{s}|x) = P_{L|X}(l|x).$$

Let

$$\mathcal{B}_k = \{b_{k,1}, b_{k,2}, \dots, b_{k,|\mathcal{B}_k|}\} = \{\Phi_v(l, \mathbf{s}) : l \in \mathcal{L}, \mathbf{s} \in \mathcal{S}^k\},$$

where for  $k = 0$ , let

$$\Phi_v(l, \mathbf{s}) = \phi_{ch}(l).$$

In addition, let  $B_k$  be a random variable taking values from  $\mathcal{B}_k$ . Then, for  $k = 0$ , we have

$$\begin{aligned} \mathcal{B}_k &= \{\phi_{ch}(l) : l \in \mathcal{L}\}, \\ P_{B_k|X}(b_{k,i}|x) &= \sum_{l \in \mathcal{L}, \phi_{ch}(l) = b_{k,i}} P_{L|X}(l|x). \end{aligned} \quad (48)$$

For  $k > 0$ , we have

$$\begin{aligned} \mathcal{B}_k &= \{\phi_v(s) + b_{k-1,j} : s \in \mathcal{S}, b_{k-1,j} \in \mathcal{B}_{k-1}\}, \\ P_{B_k|X}(b_{k,i}|x) &= \sum_{\substack{s \in \mathcal{S}, b_{k-1,j} \in \mathcal{B}_{k-1}, \\ \phi_v(s) + b_{k-1,j} = b_{k,i}}} P_{S|X}(s|x) P_{B_{k-1}|X}(b_{k-1,j}|x). \end{aligned} \quad (49)$$

---

**Algorithm 2** Computation of  $\mathcal{B}$  and  $P_{B|X}$ 

---

**Input:**  $\phi_v, \phi_{ch}, P_{S|X}, P_{L|X}, d_v$ .

**Output:**  $\mathcal{B}$  and  $P_{B|X}$ .

- 1: Set  $\mathcal{B}_k = \emptyset$  and  $P_{B_k|X}(\cdot|x) = 0$  for  $k = 0, 1, \dots, d_v - 1$  and for  $x = 0, 1$ .
  - 2: **for**  $l \in \mathcal{L}$  **do**
  - 3:    $\mathcal{B}_0 = \mathcal{B}_0 \cup \{\phi_{ch}(l)\}$ . //See (48)
  - 4:    $P_{B_0|X}(\phi_{ch}(l)|x) = P_{L|X}(l|x)$  for  $x = 0, 1$ .
  - 5: **end for**
  - 6: **for**  $k = 1, 2, \dots, d_v - 1$  **do**
  - 7:   **for**  $s \in \mathcal{S}, b_{k-1,j} \in \mathcal{B}_{k-1}$  **do**
  - 8:      $b_{k,i} = \phi_v(s) + b_{k-1,j}$ .
  - 9:      $\mathcal{B}_k = \mathcal{B}_k \cup \{b_{k,i}\}$ . //See (49)
  - 10:     $P_{B_k|X}(b_{k,i}|x) = P_{S|X}(s|x)P_{B_{k-1}|X}(b_{k-1,j}|x)$  for  $x = 0, 1$ .
  - 11:   **end for**
  - 12: **end for**
  - 13:  $P_{B|X} = P_{B_{d_v-1}|X}$ .
  - 14: **return**  $\mathcal{B}$  and  $P_{B|X}$ .
- 

*Proof:* For  $k = 0$ , (48) holds obviously. For  $k > 0$ , we have

$$\begin{aligned}\mathcal{B}_k &= \{\Phi_v(l, \mathbf{s}) : l \in \mathcal{L}, \mathbf{s} \in \mathcal{S}^k\} \\ &= \{\phi_v(s) + \Phi_v(l, \mathbf{s}) : s \in \mathcal{S}, l \in \mathcal{L}, \mathbf{s} \in \mathcal{S}^{k-1}\} \\ &= \{\phi_v(s) + b_{k-1,j} : s \in \mathcal{S}, b_{k-1,j} \in \mathcal{B}_{k-1}\};\end{aligned}$$

meanwhile, we have

$$\begin{aligned}&P_{B_k|X}(b_{k,i}|x) \\ &= \sum_{l \in \mathcal{L}, \mathbf{s} \in \mathcal{S}^k, \Phi_v(l, \mathbf{s}) = b_{k,i}} P_{L, \mathbf{S}|X}(l, \mathbf{s}|x) \\ &= \sum_{l \in \mathcal{L}, \mathbf{s} \in \mathcal{S}^k, \Phi_v(l, \mathbf{s}) = b_{k,i}} P_{L|X}(l|x) \prod_{i=1}^k P_{S|X}(s_i|x) \\ &= \sum_{s_k \in \mathcal{S}} P_{S|X}(s_k|x) \sum_{\substack{l \in \mathcal{L}, \mathbf{s} \in \mathcal{S}^{k-1}, \\ \phi_v(s_k) + \Phi_v(l, \mathbf{s}) = b_{k,i}}} P_{L|X}(l|x) \prod_{i=1}^{k-1} P_{S|X}(s_i|x) \\ &= \sum_{s_k \in \mathcal{S}} P_{S|X}(s_k|x) \sum_{\substack{l \in \mathcal{L}, \mathbf{s} \in \mathcal{S}^{k-1}, \\ \phi_v(s_k) + \Phi_v(l, \mathbf{s}) = b_{k,i}}} P_{L, \mathbf{S}|X}(l, \mathbf{s}|x) \\ &= \sum_{s \in \mathcal{S}} P_{S|X}(s|x) \sum_{\substack{b_{k-1,j} \in \mathcal{B}_{k-1}, \\ \phi_v(s) + b_{k-1,j} = b_{k,i}}} P_{B_{k-1}|X}(b_{k-1,j}|x).\end{aligned}$$

This completes the proof.  $\blacksquare$

According to Theorem 4, we can compute  $\mathcal{B}_0, P_{B_0|X}, \mathcal{B}_1, P_{B_1|X}, \dots, \mathcal{B}_{d_v-1}, P_{B_{d_v-1}|X}$  sequentially. Then,  $\mathcal{B}$  and  $P_{B|X}$  equal to  $\mathcal{B}_{d_v-1}$  and  $P_{B_{d_v-1}|X}$ , respectively. We summarize the computation by Algorithm 2. Since  $|\mathcal{B}_{k-1}|$  in line 7 of Algorithm 2 is upper-bounded by  $2^{q_v}$ , the complexity of Algorithm 2 is  $O(d_v 2^{q_v} |\mathcal{S}|)$ .

At this point, starting from  $\mathcal{B}$  and  $P_{B|X}$ , we can compute the optimal SDQ  $\Lambda_v$  given by (33). The computational complexity

is upper-bounded by  $O(2^{2q_v} |\mathcal{R}|)$  [15], [16]. For the special situation where  $P_{B|X}$  satisfies

$$\frac{P_{B|X}(b_1|0)}{P_{B|X}(b_1|1)} \geq \frac{P_{B|X}(b_2|0)}{P_{B|X}(b_2|1)} \geq \dots \geq \frac{P_{B|X}(b_{|\mathcal{B}|}|0)}{P_{B|X}(b_{|\mathcal{B}|}|1)}, \quad (50)$$

the computational complexity can be reduced to  $O(2^{q_v} |\mathcal{R}|)$  [16], [20]. The simulation results show that (50) frequently holds. This phenomenon is reasonable because  $\phi_v = \phi_v^*$  and  $\phi_{ch} = \phi_{ch}^*$  can always make (50) hold according to (55), while we set  $\phi_v$  and  $\phi_{ch}$  by scaling  $\phi_v^*$  and  $\phi_{ch}^*$ , respectively (see (45)). After the computation of  $\Lambda_v$ , we can then compute the TS  $\Gamma_v$ , the UF  $Q_v$ , and the pmf  $P_{R|X}$  given by (34), (35), and (36) respectively. Till now, the MIM-QBP decoder design at VN is completed, which has a total complexity upper-bounded by  $O(d_v 2^{q_v} |\mathcal{S}| + 2^{2q_v} |\mathcal{R}|)$  (for one decoding iteration).

After the design of the MIM-QBP decoder at VN, we can use the hardware architecture shown by Fig. 10 to implement the update at VN for computing all outgoing messages  $r_1, r_2, \dots, r_{d_v}$ . The computational complexity is  $O(d_v + d_v \lceil \log_2(|\mathcal{R}|) \rceil)$  for one VN for one iteration, where  $O(d_v)$  refers to the complexity of addition operations, and  $O(d_v \lceil \log_2(|\mathcal{R}|) \rceil)$  refers to the complexity of mapping operations based on  $\Gamma_v$  for the  $d_v$  outgoing messages.

### C. Remarks

As illustrated by Section III-D, the design of  $Q_e$  is quite similar to that of  $Q_v$ . In particular, the same RFs  $\phi_v$  and  $\phi_{ch}$  can be used for the design of  $Q_e$  and  $Q_v$  for a same decoding iteration, essentially because we can derive a theorem similar to Theorem 3 for the design of  $Q_e$ . In addition, the condition of (47) ensures that the additions involved in the design of  $Q_e$  do not overflow. Moreover, we can also derive a theorem similar to Theorem 4 and an algorithm similar to Algorithm 2 for the design of  $Q_e$ . At this point, the design of  $Q_e$  is clear, which has a complexity of  $O(d_v 2^{q_v} |\mathcal{S}| + 2^{2q_v} |\mathcal{X}|)$  (for one decoding iteration). After the design of  $Q_e$ , implementing  $Q_e$  for one VN for one iteration during decoding has complexity  $O(d_v)$ , which is the complexity of addition operations.

We have finished illustrating how to practically design the MIM-QBP decoder given the parameters  $P_{L|X}, \mathcal{L}, \mathcal{R}, \mathcal{S}, q_c$ , and  $q_v$ . Like the MIM-LUT decoder, the quality of the MIM-QBP decoder also heavily depends on the choice of  $P_{L|X}$ , which is essentially determined by the design noise standard deviation  $\sigma_d$ . Our simulation results indicate that a good  $\sigma_d$  should also be around the decoding threshold  $\sigma^*$ . It is interesting that both the MIM-LUT decoder and the the MIM-QBP decoder can be designed at a certain  $\sigma_d$  around  $\sigma^*$  while working very well at all noise levels (noise standard deviations). It may be counter-intuitive that for any noise level  $\sigma$  not around  $\sigma^*$ , the decoder designed at  $\sigma_d = \sigma$  generally work very bad even at the noise level  $\sigma$  according to extensive simulation results. The essential reason for this phenomenon has not been reported at this moment.

Since the MIM-LUT decoder [7]–[14] only uses table lookup operations during decoding, the addition operations may be regarded as a shortcoming of the MIM-QBP decoder.

However, thanks to the use of additions, the MIM-QBP decoder can overcome the shortcoming of the MIM-LUT decoder due to using LUTs (either large memory requirement or information loss resulted from decomposition). Moreover, additions lead to MIM-QBP decoder simple hardware architectures shown by Figures 9 and 10 for implementing the CN and VN update, respectively. In contrast, the MIM-LUT decoding currently seems not to have a general simple architecture for implementing its node update [21].

To end this section, we explain why we name our proposed decoder the MIM-QBP decoder. On the one hand, our decoder is essentially derived by scaling  $\phi_c^*$  given by (37) and  $\phi_v^*, \phi_{ch}^*$  given by (44). According to Corollaries 1 and 2,  $\phi_c = \eta_1 \phi_c^*, \phi_v = \eta_2 \phi_v^*$ , and  $\phi_{ch} = \eta_2 \phi_{ch}^*$  can maximize the MI between the channel input and each node's output, where  $\eta_1$  and  $\eta_2$  are two positive numbers. This is what the term "MIM" refers to. On the other hand, as mentioned before, we closely relate our decoder to the BP decoder when considering design the RFs. In fact, our decoder works on finite alphabets in which the symbols can be regarded as the quantization outputs of messages associated with LLRs, while the BP algorithm directly works on messages represented by LLRs. This is what the term "QBP" refers to.

## V. MIM-QBP DECODING OF IRREGULAR LDPC CODES

In this section, we derive the MIM-QBP decoding of irregular LDPC codes. This section is carried out largely based on the previous three sections which discuss the MIM-QBP decoding of regular LDPC codes. We will devote many efforts to illustrate the correlation between regular and irregular MIM-QBP LDPC decoding.

Denote  $\mathcal{D}_c = \{d_{c,1}, d_{c,2}, \dots, d_{c,max}\}$  with  $d_{c,1} < d_{c,2} < \dots < d_{c,max}$  and  $\mathcal{D}_v = \{d_{v,1}, d_{v,2}, \dots, d_{v,max}\}$  with  $d_{v,1} < d_{v,2} < \dots < d_{v,max}$  as the sets formed by CN and VN degrees, respectively. For convenience, let  $\mathcal{D}'_c = \{i-1 : i \in \mathcal{D}_c\}$  and  $\mathcal{D}'_v = \{i-1 : i \in \mathcal{D}_v\}$ . Denote

$$\rho(x) = \sum_{i \in \mathcal{D}_c} \rho_i x^{i-1} \text{ and } \theta(x) = \sum_{i \in \mathcal{D}_v} \theta_i x^{i-1}$$

as the CN and VN degree distributions, where  $\rho_i$  and  $\theta_i$  are the fractions of edges incident to degree- $i$  CNs and VNs, respectively. For any set  $\mathcal{U}$  and any integer set  $\mathcal{V}$ , denote  $\mathcal{U}^\mathcal{V} = \cup_{i \in \mathcal{V}} \mathcal{U}^i$ . We now illustrate the MIM-QBP decoder design at CN and VN for irregular LDPC codes.

### A. Irregular MIM-QBP Decoder Design at CN

For the CN update for irregular LDPC codes, since the outgoing edge connects to a degree- $i$  CN at probability  $\rho_i$ , the incoming message  $\mathbf{R} \in \mathcal{R}^{\mathcal{D}'_c}$  takes  $\dim(\mathbf{R}) = i \in \mathcal{D}'_c$  with probability  $\rho_{i+1}$ . Then, the UF

$$Q_c : \mathcal{R}^{\mathcal{D}'_c} \rightarrow \mathcal{S}$$

is used for the CN update for irregular LDPC codes, which includes the UF (4) for regular LDPC codes as a subcase when  $|\mathcal{D}'_c| = 1$ . We also design  $Q_c$  to maximize  $I(X; S)$ .

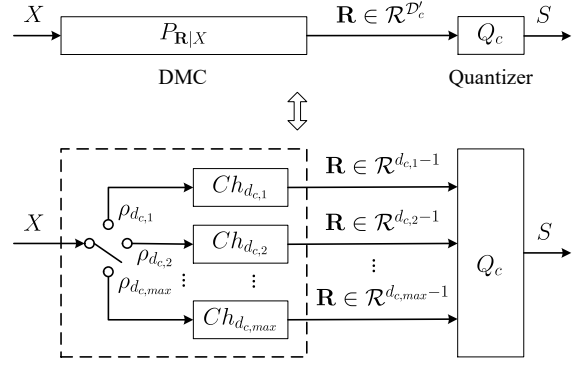


Fig. 11. Quantization of a discrete memoryless channel (DMC), where the quantizer works exactly the same as the check node update function  $Q_c$  for the mutual information-maximizing lookup table (MIM-LUT) decoding for the irregular LDPC code with check node degree distribution  $\rho(x) = \sum_{d_{c,i} \in \mathcal{D}_c} \rho_{d_{c,i}} x^{i-1}$ . For  $d_{c,i} \in \mathcal{D}_c$ , the switch connects to the channel  $Ch_{d_{c,i}}$  at probability  $\rho_{d_{c,i}}$ , where the channel  $Ch_{d_{c,i}}$  refers to the channel shown by Fig. 4 with  $d_c = d_{c,i}$ .

This design problem is equivalent to the DMC quantization problem shown by Fig. 11.

The joint distribution  $P_{\mathbf{R}|X}(\mathbf{r}|x)$  of  $\mathbf{R}$  conditioned on the channel input bit  $X$  at a CN (i.e., the channel transition probability  $P_{\mathbf{R}|X}(\mathbf{r}|x)$  with respect to the DMC shown by Fig. 11) is given by

$$P_{\mathbf{R}|X}(\mathbf{r}|x) = \rho_{\dim(\mathbf{r})+1} \left( \frac{1}{2} \right)^{\dim(\mathbf{r})-1} \sum_{\mathbf{x}: \oplus \mathbf{x} = x} \prod_{i=1}^{\dim(\mathbf{r})} P_{\mathbf{R}|X}(r_i|x_i).$$

With each incoming message realization  $\mathbf{r} \in \mathcal{R}^{d_c-1}$  replaced by  $\mathbf{r} \in \mathcal{R}^{\mathcal{D}'_c}$ , we can totally reuse Section III-B to illustrate the MIM-QBP decoder design at a CN of irregular LDPC codes.

We now illustrate how to practically design the MIM-QBP decoder at a CN of irregular LDPC codes following Section IV-A. Let  $\epsilon$  used in (37) satisfy ( $d_c$  is replaced by  $d_{c,max}$ )

$$0 < \epsilon d_{c,max} < \min \{ |\log(|g(\mathbf{r})|)| - \log(|g(\mathbf{r}')|)| \}$$

$$\mathbf{r}, \mathbf{r}' \in \mathcal{R}^{\mathcal{D}'_c}, g(\mathbf{r}) \neq g(\mathbf{r}'), \text{sgn}(g(\mathbf{r})) = \text{sgn}(g(\mathbf{r}')) \neq 0 \}.$$

We can similarly prove Theorem 1 and Corollary 1 (replacing  $\mathcal{R}^{d_c-1}$  with  $\mathcal{R}^{\mathcal{D}'_c}$ ) for irregular MIM-QBP decoder. Accordingly, we can practically design the RF  $\phi_c$  based on (39) with  $|\phi_c|_{max} = \lfloor (2^{q_c-1} - 1) / d_{c,max} \rfloor$ . Furthermore, since Theorem 2 still holds, we can use Algorithm 1 to compute  $\mathcal{A}_i$  and  $P_{\mathcal{A}_i|X}$  for  $i \in \mathcal{D}'_c$  with a total complexity of  $O(d_{c,max} 2^{q_c} |\mathcal{R}|)$ . Then, for irregular MIM-QBP decoder, we have

$$\mathcal{A} = \cup_{i \in \mathcal{D}'_c} \mathcal{A}_i, \\ P_{\mathcal{A}|X}(a|x) = \sum_{i \in \mathcal{D}'_c} \rho_{i+1} P_{\mathcal{A}_i|X}(a|x).$$

Next, starting from  $\mathcal{A}$  and  $P_{\mathcal{A}|X}$ , we can sequentially compute the optimal SDQ  $\Lambda_c$ , the TS  $\Gamma_c$ , the UF  $Q_c$ , and the pmf  $P_{S|X}$  given by (22)–(25), respectively. Till now, the MIM-QBP

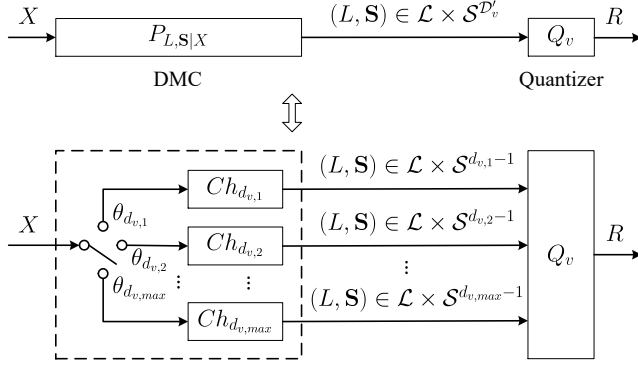


Fig. 12. Quantization of a discrete memoryless channel (DMC), where the quantizer works exactly the same as the variable node update function  $Q_v$  for the mutual information-maximizing lookup table (MIM-LUT) decoding for the irregular LDPC code with variable node degree distribution  $\theta(x) = \sum_{d_{v,i} \in \mathcal{D}_v} \theta_{d_{v,i}} x^{i-1}$ . For  $d_{v,i} \in \mathcal{D}_v$ , the switch connects to the channel  $Ch_{d_{v,i}}$  at probability  $\theta_{d_{v,i}}$ , where the channel  $Ch_{d_{v,i}}$  refers to the channel shown by Fig. 5 with  $d_v = d_{v,i}$ .

decoder design at CNs of irregular LDPC codes is completed, having a total complexity of  $O(d_{c,max} 2^{q_c} |\mathcal{R}| + 2^{2q_c} |\mathcal{S}|)$  (for one decoding iteration).

### B. Irregular MIM-QBP Decoder Design at VN

For the VN update for irregular LDPC codes, since the outgoing edge connects to a degree- $i$  VN at probability  $\theta_i$ , the incoming message  $(L, \mathbf{S}) \in \mathcal{L} \times \mathcal{S}^{\mathcal{D}'_v}$  takes  $\dim(\mathbf{S}) = i \in \mathcal{D}'_v$  with probability  $\theta_{i+1}$ . Then, the UF

$$Q_v : \mathcal{L} \times \mathcal{S}^{\mathcal{D}'_v} \rightarrow \mathcal{R}$$

is used for the VN update for irregular LDPC codes, which includes the UF (8) for regular LDPC codes as a subcase when  $|\mathcal{D}'_v| = 1$ . We also design  $Q_v$  to maximize  $I(X; R)$ . This design problem is equivalent to the DMC quantization problem shown by Fig. 12.

The joint distribution  $P_{L, \mathbf{S}|X}(l, \mathbf{s}|x)$  of  $(L, \mathbf{S})$  conditioned on the channel input bit  $X$  at a VN (i.e., the channel transition probability  $P_{L, \mathbf{S}|X}(l, \mathbf{s}|x)$  with respect to the DMC shown by Fig. 12) is given by

$$P_{L, \mathbf{S}|X}(l, \mathbf{s}|x) = \theta_{\dim(\mathbf{s})+1} P_{L|X}(l|x) \prod_{i=1}^{\dim(\mathbf{s})} P_{S_i|X}(s_i|x).$$

With each incoming message realization  $(l, \mathbf{s}) \in \mathcal{L} \times \mathcal{S}^{d_v-1}$  replaced by  $(l, \mathbf{s}) \in \mathcal{L} \times \mathcal{S}^{\mathcal{D}'_v}$ , we can totally reuse Section III-C to illustrate the MIM-QBP decoder design at a VN of irregular LDPC codes.

We now illustrate how to practically design the MIM-QBP decoder at a VN of irregular LDPC codes following Section IV-B. We can similarly prove Theorem 3 and Corollary 2 (replacing  $\mathcal{L} \times \mathcal{S}^{d_v-1}$  with  $\mathcal{L} \times \mathcal{S}^{\mathcal{D}'_v}$ ) for irregular MIM-QBP decoder. Accordingly, we can practically design the RFs  $\phi_v$  and  $\phi_{ch}$  based on (45) with  $|\phi_{v,ch}|_{max} = \lfloor (2^{q_v-1} - 1)/d_{v,max} \rfloor$ . Furthermore, since Theorem 4 still holds, we can use Algorithm 2 to compute  $\mathcal{B}_i$  and  $P_{B_i|X}$  for  $i \in \mathcal{D}'_v$  with

a total complexity of  $O(d_{v,max} 2^{q_v} |\mathcal{S}|)$ . Then, for irregular MIM-QBP decoder, we have

$$\mathcal{B} = \cup_{i \in \mathcal{D}'_v} \mathcal{B}_i, \\ P_{B|X}(b|x) = \sum_{i \in \mathcal{D}'_v} \theta_{i+1} P_{B_i|X}(b|x).$$

The computation of  $\mathcal{A}, \mathcal{B}, P_{A|X}$ , and  $P_{B|X}$  may give the biggest difference between the practical design of MIM-QBP decoder for regular and irregular LDPC codes. Next, we can sequentially compute the optimal SDQ  $\Lambda_v$ , the TS  $\Gamma_v$ , the UF  $Q_v$ , and the pmf  $P_{R|X}$  given by (33)–(36), respectively. Till now, the MIM-QBP decoder design at VNs of irregular LDPC codes is completed, having a total complexity of  $O(d_{v,max} 2^{q_v} |\mathcal{S}| + 2^{2q_v} |\mathcal{R}|)$  (for one decoding iteration).

### C. Remarks

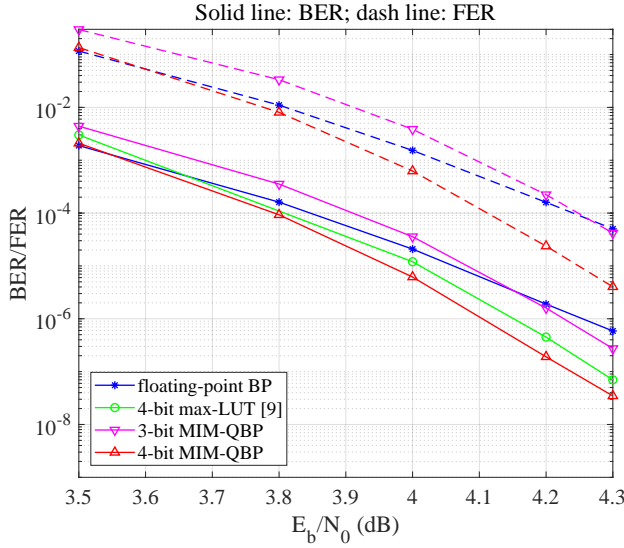
Instead of using (11), the estimation function

$$Q_e : \mathcal{L} \times \mathcal{S}^{\mathcal{D}_v} \rightarrow \mathcal{X}$$

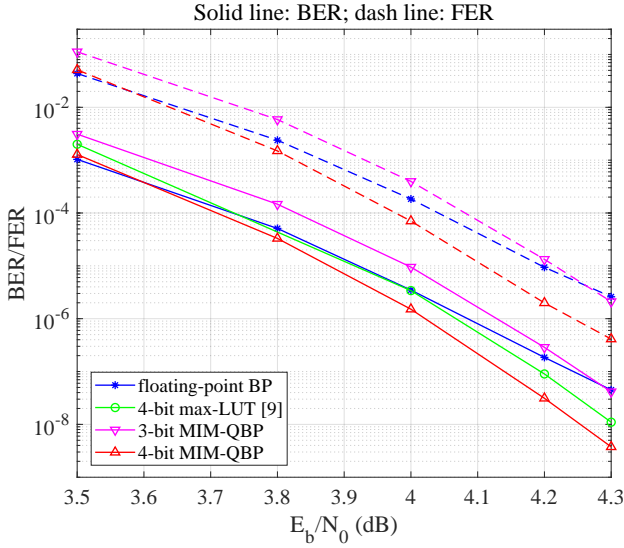
is used to estimate the channel input bit corresponding to each VN for irregular LDPC codes. We still ignore the details since the design of  $Q_e$  is quite similar to the design of  $Q_v$ .

We now compare the design of the irregular MIM-LUT decoder with the design of the irregular MIM-LUT decoder [13], [14]. The idea for designing the irregular MIM-LUT decoder can be analogously shown by Figures 11 and 12, where a joint design is considered over all sub-channels (i.e., the channels labelled by “ $Ch_{d_{c,i}}$ ” and “ $Ch_{d_{v,i}}$ ”), with each sub-channel referring to the design at a node with a specific degree. Since a single LUT for storing the UFs/quantizers  $Q_c$  and  $Q_v$  is unpractical, the authors of [13] and [14] apply individual design to each sub-channel to reduce its output size. This individual design coincides with the design for regular MIM-LUT decoder, as explained in previous sections, where the decomposition technique is employed to avoid memory overflow. After the individual design, each sub-channel has a manageable output, like  $\mathcal{S}$  and  $\mathcal{R}$  in [14], and then the joint design can be taken over all sub-channels. Obviously, the individual design will deteriorate the performance of the irregular MIM-LUT decoder, and different sub-channels result in different LUTs. Instead, the MIM-QBP decoder has no problem on dealing with all sub-channels’ original output  $\mathcal{R}^{\mathcal{D}'_c}$  and  $\mathcal{L} \times \mathcal{S}^{\mathcal{D}'_v}$ , and the same RFs and TSs can be used for different sub-channels i.e., for the update at nodes with different degrees.

During the decoding process of the irregular MIM-QBP decoder, the simple hardware architecture shown by Fig. 9 (resp. Fig. 10) can be used to implement the CN (resp. VN) update for computing all outgoing messages from this node. The average computational complexity is  $O(\sum_{i \in \mathcal{D}'_c} \rho_i (i + i \lceil \log_2(|\mathcal{S}|) \rceil))$  (resp.  $O(\sum_{i \in \mathcal{D}'_v} \theta_i (i + i \lceil \log_2(|\mathcal{R}|) \rceil))$ ) for one CN (resp. VN) for one iteration.



(a) A maximum of 10 iterations.



(b) A maximum of 30 iterations.

Fig. 13. BER and FER results for the (6, 32) code [22] of length 2048 and rate 0.84. Results for the max-LUT decoder are from [9, Fig. 5]. We set  $(q_c, q_v) = (10, 8)$  and  $(q_c, q_v) = (12, 10)$  for the 3- and 4-bit MIM-QBP decoders, respectively.

## VI. SIMULATION RESULTS

We use Monte-Carlo simulation to estimate decoders' error performances, assuming binary phase-shift keying (BPSK) transmission over the AWGN channel. We design the MIM-QBP decoder by fixing  $|\mathcal{L}| = |\mathcal{R}| = |\mathcal{S}| = 8/16$  (3-/4-bit decoder) for all iterations. We will specify  $q_c$ ,  $q_v$ , and  $\sigma_d$  for each simulation example. In addition, at least 100 frame errors are collected for each simulated SNR point.

### A. Regular Codes

*Example 3:* Consider the regular (6, 32) LDPC code taken from [22]. This code has length 2048 and rate 0.84. We

TABLE III  
RECONSTRUCTION FUNCTION  $\phi_c$  OF THE 3-BIT MIM-QBP DECODER IN EXAMPLE 3

iteration	$\phi_c(\cdot)$							
	0	1	2	3	4	5	6	7
1	1	1	4	15	-15	-4	-1	-1
2	1	1	3	15	-11	-3	-1	-1
3	1	1	3	10	-15	-3	-1	-1
4	1	1	3	15	-10	-3	-1	-1
5-7	1	1	3	10	-15	-3	-1	-1
8	1	1	4	15	-12	-3	-1	-1
9-10	1	1	3	11	-15	-3	-1	-1

TABLE IV  
RECONSTRUCTION FUNCTION  $\phi_v$  OF THE 3-BIT MIM-QBP DECODER IN EXAMPLE 3

iteration	$\phi_v(\cdot)$							
	0	1	2	3	4	5	6	7
1	4	2	1	0	0	-1	-2	-4
2	4	2	1	0	-1	-2	-3	-5
3	5	3	1	0	-1	-2	-3	-5
4-7	5	3	2	1	0	-1	-3	-5
8	5	3	1	0	-1	-2	-3	-5
9-10	5	3	2	1	0	-1	-3	-5

use  $(q_c, q_v) = (10, 8)/(12, 10)$  to design the 3-/4-bit MIM-QBP decoder at  $\sigma_d = 0.5343/0.5417$ , respectively. Different decoders' bit error rates (BERs) and frame error rates (FERs) are presented by Fig. 13.

We show the details of the 3-bit MIM-QBP decoder used for the simulations in Fig. 13(a). These details can be used for reference when using our method to design the 3-bit MIM-QBP decoder with  $(q_c, q_v) = (10, 8)$  at  $\sigma_d = 0.5343$ . The 7 thresholds used for quantizing the AWGN channel (see Section II-A) are

$$\{-0.702, -0.39, -0.18, 0, 0.18, 0.39, 0.702\}.$$

The RFs  $\phi_c$ ,  $\phi_v$ , and  $\phi_{ch}$  are given by Tables III, IV, and V, respectively. The TSs  $\Gamma_c$  and  $\Gamma_v$  are given by Tables VI and VII, respectively. The TSs  $\Gamma_e = \{\gamma_1\}$  for the estimation function  $Q_e$  for iterations 1 to 10 are

$$\gamma_1 = 0, 1, 0, 1, 1, 1, 1, 1, 1, 1,$$

respectively.

From Tables IV and V, we can see that 7 bits are enough for implementing the additions at VN for the 3-bit MIM-QBP decoder with a maximum of 10 iterations. We have illustrated how to save resource or make full use of the  $q_v = 8$  bits around (47).  $\square$

*Example 4:* Consider the regular (4, 36) LDPC code with identifier 1998.5.3.2665 taken from [23]. This code has length 1998 and rate 0.89. We use  $q_c = q_v = 12$  to design the 3-/4-

TABLE V  
RECONSTRUCTION FUNCTION  $\phi_{ch}$  OF THE 3-BIT MIM-QBP DECODER IN  
EXAMPLE 3

iteration	$\phi_{ch}(\cdot)$							
	0	1	2	3	4	5	6	7
1–10	18	10	5	2	–2	–5	–10	–18

TABLE VI  
THRESHOLD SET  $\Gamma_c$  OF THE 3-BIT MIM-QBP DECODER IN EXAMPLE 3

iteration	$\gamma_1$	$\gamma_2$	$\gamma_3$	$\gamma_4$	$\gamma_5$	$\gamma_6$	$\gamma_7$
1	34	40	51	76	–55	–43	–37
2	33	37	49	–51	–39	–35	–33
3	31	35	47	–50	–39	–35	–33
4–6	31	33	37	49	–48	–37	–33
7	31	33	40	54	–46	–37	–33
8	31	37	51	–52	–40	–35	–33
9–10	31	33	37	51	–49	–37	–33

TABLE VII  
THRESHOLD SET  $\Gamma_v$  OF THE 3-BIT MIM-QBP DECODER IN EXAMPLE 3

iteration	$\gamma_1$	$\gamma_2$	$\gamma_3$	$\gamma_4$	$\gamma_5$	$\gamma_6$	$\gamma_7$
1	13	7	3	0	–3	–7	–13
2	14	8	4	1	–2	–6	–12
3	13	7	3	0	–3	–7	–13
4–10	14	8	4	1	–2	–6	–12

bit MIM-QBP decoder at  $\sigma_d = 0.4801/0.4899$ , respectively. Different decoders' BERs are presented by Fig. 14.  $\square$

*Example 5:* Consider the regular (3, 6) LDPC code with identifier 8000.4000.3.483 taken from [23]. This code has length 8000 and rate 0.5. We use  $(q_c, q_v) = (9, 8)/(10, 10)$  to design the 3-/4-bit MIM-QBP decoder at  $\sigma_d = 0.8479/0.8660$ , respectively. Different decoders' BERs are presented by Fig. 15. Note that the 3-/4-bit non-uniform QBP decoder taken from [5] requires  $(q_c, q_v) = (9, 8)/(12, 10)$ , respectively.  $\square$

### B. Irregular Codes

*Example 6:* Consider the three irregular codes  $\mathcal{C}_1, \mathcal{C}_2$ , and  $\mathcal{C}_3$  whose CN degree distributions are given by

$$\begin{aligned}\rho^{(1)}(x) &= 0.052632x^6 + 0.902256x^7 + 0.045113x^8, \\ \rho^{(2)}(x) &= 0.32338x^7 + 0.67662x^8, \\ \rho^{(3)}(x) &= 0.372093x^7 + 0.627907x^8,\end{aligned}$$

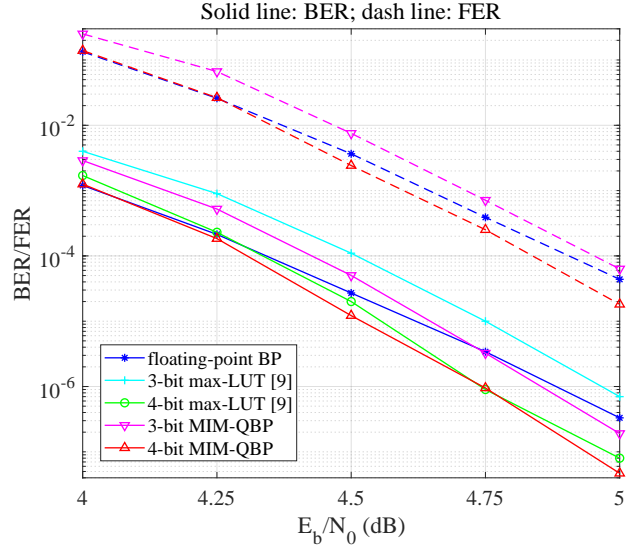


Fig. 14. BER and FER results for the (4, 36) code (with identifier 1998.5.3.2665 in [23]) of length 1998 and rate 0.89. A maximum of 10 iterations is used. Results for the max-LUT decoders are from [9, Fig. 4]. We set  $q_c = q_v = 12$  for the MIM-QBP decoders.

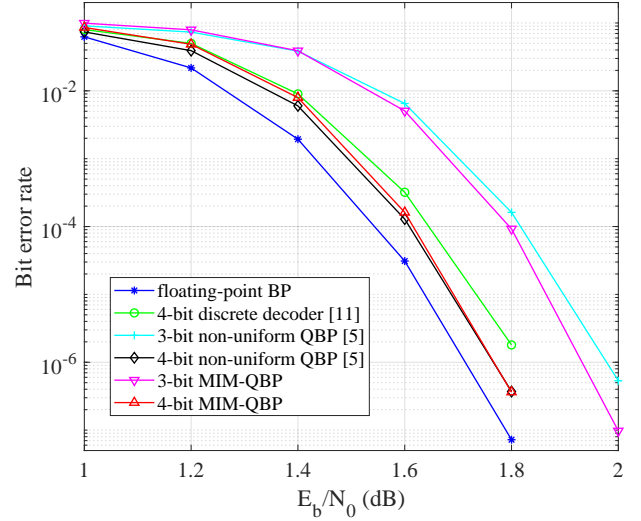


Fig. 15. BER results for the (3, 6) code (with identifier 8000.4000.3.483 in [23]) of length 8000 and rate 0.5. A maximum of 50 iterations is used. Results for the discrete decoder are from [11, Fig. 18]. We set  $(q_c, q_v) = (9, 8)$  and  $(q_c, q_v) = (10, 10)$  for the 3- and 4-bit MIM-QBP decoders, respectively.

and VN degree distributions are given by

$$\begin{aligned}\theta^{(1)}(x) &= 0.240602x + 0.210526x^2 + 0.030075x^3 + \\ &\quad 0.125313x^4 + 0.017544x^6 + 0.375940x^{14}, \\ \theta^{(2)}(x) &= 0.13805x + 0.40104x^2 + \\ &\quad 0.02659x^8 + 0.43433x^{16}, \\ \theta^{(3)}(x) &= 0.139535x + 0.404651x^2 + \\ &\quad 0.020930x^8 + 0.434884x^{16},\end{aligned}$$

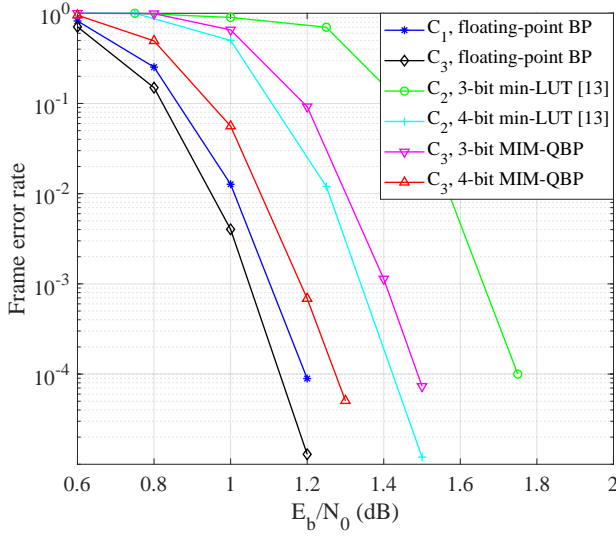


Fig. 16. FER results for the irregular codes  $\mathcal{C}_1, \mathcal{C}_2$ , and  $\mathcal{C}_3$  of length 10000 and rate 0.5 (see Example 6 for codes' degree distributions). A maximum of 100 iterations is used. Results for the min-LUT decoders are from [13, Fig. 3]. We set  $q_c = q_v = 12$  for the 3-4-bit MIM-QBP decoder.

respectively. The three codes have length 10000 and rate 0.5. Both of  $\mathcal{C}_1$  and  $\mathcal{C}_3$ 's parity-check matrices consist of a  $50 \times 100$  array of  $100 \times 100$  circulants and are constructed by using the one-edge metric-constrained quasi-cyclic progressive edge-growth algorithm [24].

$\mathcal{C}_1$  is optimized for the BP decoder.  $\mathcal{C}_2$  was optimized by [13] for the irregular MIM-LUT decoder proposed by [13], because the MIM-LUT decoder can not perform well when testing on  $\mathcal{C}_1$ . We have observed that the MIM-QBP decoder also can not perform well when testing on  $\mathcal{C}_1$ . To fairly compare with the irregular MIM-LUT decoder, we test the MIM-QBP decoder on  $\mathcal{C}_3$  which has similar code parameters with  $\mathcal{C}_2$ . We use  $q_c = q_v = 12$  to design the 3-4-bit MIM-QBP decoder at  $\sigma_d = 0.8989/0.9290$ , respectively. Different decoders' FERs are presented by Fig. 16.  $\square$

## VII. CONCLUSION

In this paper, we have proposed a method to remove the tables used for MIM-LUT decoding [7]–[14] so as to greatly save memory costs. Our method leads to the hardware-friendly MIM-QBP decoder which can be implemented based only on simple mappings and fixed-point additions. From this point of view, our decoder works similarly to those presented by [4]–[6], but instead of using hand optimization, we have shown how to practically and systematically design the MIM-QBP decoder for both regular and irregular LDPC codes. Simulation results show that the MIM-QBP decoder can always considerably outperform the state-of-the-art MIM-LUT decoder [7]–[14]. Moreover, in terms of error performance, the MIM-QBP decoder has advantages over the floating-point BP decoder when

- the maximum allowed number of decoding iterations is small (generally less than 30), and/or

- the code rate is high, and/or
- the operating SNR is high.

In particular, as can be seen from Figures 13 and 14, even the 3-bit MIM-QBP decoder can outperform the floating-point BP decoder at high SNR region when testing on high rate codes with a maximum of 10–30 iterations.

## APPENDIX A PROOF OF THEOREM 1

Let  $\phi_c = \phi_c^*$ . For  $\mathbf{r} \in \mathcal{R}^{d_c-1}$ , we have

$$g(\mathbf{r}) = \prod_{i=1}^{\dim(\mathbf{r})} g(r_i)$$

according to (6). Let

$$h(\mathbf{r}) = |\{r_i : 1 \leq i \leq \dim(\mathbf{r}), |g(r_i)| = 1\}|.$$

Then, we have

$$\begin{aligned} |\Phi_c(\mathbf{r})| &= \sum_{i=1}^{\dim(\mathbf{r})} |\phi_c^*(r_i)| \\ &= - \sum_{i=1}^{\dim(\mathbf{r})} \log(|g(r_i)|) + h(\mathbf{r})\epsilon \\ &= - \log \left( \prod_{i=1}^{\dim(\mathbf{r})} |g(r_i)| \right) + h(\mathbf{r})\epsilon \\ &= - \log(|g(\mathbf{r})|) + h(\mathbf{r})\epsilon. \end{aligned} \quad (51)$$

Meanwhile, we have

$$\begin{aligned} \text{sgn}(\Phi_c(\mathbf{r})) &= \prod_{i=1}^{\dim(\mathbf{r})} \text{sgn}(\phi_c(r_i)) \\ &= \prod_{i=1}^{\dim(\mathbf{r})} \text{sgn}(g(r_i)) = \text{sgn}(g(\mathbf{r})). \end{aligned} \quad (52)$$

For  $\mathbf{r}, \mathbf{r}' \in \mathcal{R}^{d_c-1}$ , assume  $\Phi_c(\mathbf{r}) = a_i$  and  $\Phi_c(\mathbf{r}') = a_{i'}$ , we are now to prove

$$\frac{P_{\mathbf{R}|X}(\mathbf{r}|0)}{P_{\mathbf{R}|X}(\mathbf{r}|1)} > \frac{P_{\mathbf{R}|X}(\mathbf{r}'|0)}{P_{\mathbf{R}|X}(\mathbf{r}'|1)} \Rightarrow i < i'. \quad (53)$$

we have

$$\begin{aligned} P_{\mathbf{R}|X}(\mathbf{r}|0)/P_{\mathbf{R}|X}(\mathbf{r}|1) &> P_{\mathbf{R}|X}(\mathbf{r}'|0)/P_{\mathbf{R}|X}(\mathbf{r}'|1) \\ \Rightarrow P_{X|\mathbf{R}}(0|\mathbf{r})/P_{X|\mathbf{R}}(1|\mathbf{r}) &> P_{X|\mathbf{R}}(0|\mathbf{r}')/P_{X|\mathbf{R}}(1|\mathbf{r}') \\ \Rightarrow g(\mathbf{r}) &> g(\mathbf{r}') \end{aligned}$$

If  $\text{sgn}(g(\mathbf{r})) \neq \text{sgn}(g(\mathbf{r}'))$ , we have

$$\begin{aligned} P_{\mathbf{R}|X}(\mathbf{r}|0)/P_{\mathbf{R}|X}(\mathbf{r}|1) &> P_{\mathbf{R}|X}(\mathbf{r}'|0)/P_{\mathbf{R}|X}(\mathbf{r}'|1) \\ \Rightarrow \text{sgn}(g(\mathbf{r})) &> \text{sgn}(g(\mathbf{r}')) \\ \stackrel{(a)}{\Rightarrow} \text{sgn}(\Phi_c(\mathbf{r})) &> \text{sgn}(\Phi_c(\mathbf{r}')) \\ \Rightarrow \Phi_c(\mathbf{r}) &\succ \Phi_c(\mathbf{r}') \\ \stackrel{(b)}{\Rightarrow} i &< i', \end{aligned}$$



where (a) and (b) are based on (52) and (20). Otherwise, we have  $\text{sgn}(g(\mathbf{r})) = \text{sgn}(g(\mathbf{r}')) \neq 0$ , leading to

$$\begin{aligned}
& P_{\mathbf{R}|X}(\mathbf{r}|0)/P_{\mathbf{R}|X}(\mathbf{r}|1) > P_{\mathbf{R}|X}(\mathbf{r}'|0)/P_{\mathbf{R}|X}(\mathbf{r}'|1) \\
& \Rightarrow \text{sgn}(g(\mathbf{r}))|g(\mathbf{r})| > \text{sgn}(g(\mathbf{r}'))|g(\mathbf{r}')| \\
& \Rightarrow -\text{sgn}(g(\mathbf{r}))\log(|g(\mathbf{r})|) < -\text{sgn}(g(\mathbf{r}'))\log(|g(\mathbf{r}')|) \\
& \stackrel{(c)}{\Rightarrow} \text{sgn}(g(\mathbf{r}))(-\log(|g(\mathbf{r})|) + h(\mathbf{r})\epsilon) < \\
& \quad \text{sgn}(g(\mathbf{r}'))(-\log(|g(\mathbf{r}')|) + h(\mathbf{r}')\epsilon) \\
& \stackrel{(d)}{\Rightarrow} \Phi_c(\mathbf{r}) < \Phi_c(\mathbf{r}') \\
& \Rightarrow \Phi_c(\mathbf{r}) \succ \Phi_c(\mathbf{r}') \\
& \stackrel{(e)}{\Rightarrow} i < i',
\end{aligned}$$

where (c), (d) and (e) are based on (38), (51), and (20), respectively. At this point, the proof of (53) is completed.

(53) implies that elements in  $\mathcal{A}$  are listed in a way (see (20)) equivalent to listing  $\mathbf{r} \in \mathcal{R}^{d_c-1}$  in descending order based on  $P_{\mathbf{R}|X}(\mathbf{r}|0)/P_{\mathbf{R}|X}(\mathbf{r}|1)$  (see (2)). Therefore,  $Q_c$  defined by (24) can maximize  $I(X; S)$  among all the functions mapping  $\mathcal{R}^{d_c-1}$  to  $\mathcal{S}$  according to Section II-A.

#### APPENDIX B PROOF OF THEOREM 3

Let  $\phi_v = \phi_v^*$  and  $\phi_{ch} = \phi_{ch}^*$ . For  $(l, \mathbf{s}) \in \mathcal{L} \times \mathcal{S}^{d_v-1}$ , according to (29), we have

$$\Phi_v(l, \mathbf{s}) = \log \left( \frac{P_{L|X}(l|0)}{P_{L|X}(l|1)} \prod_{i=1}^{\dim(\mathbf{s})} \frac{P_{S|X}(s_i|0)}{P_{S|X}(s_i|1)} \right). \quad (54)$$

Then, for  $(l, \mathbf{s}), (l', \mathbf{s}') \in \mathcal{L} \times \mathcal{S}^{d_v-1}$ , assume  $\Phi_v(l, \mathbf{s}) = b_i$  and  $\Phi_v(l', \mathbf{s}') = b_{i'}$ . We have

$$\begin{aligned}
& \frac{P_{L,S|X}(l, \mathbf{s}|0)}{P_{L,S|X}(l, \mathbf{s}|1)} > \frac{P_{L,S|X}(l', \mathbf{s}'|0)}{P_{L,S|X}(l', \mathbf{s}'|1)} \\
& \stackrel{(f)}{\Rightarrow} \frac{P_{L|X}(l|0)}{P_{L|X}(l|1)} \prod_{i=1}^{\dim(\mathbf{s})} \frac{P_{S|X}(s_i|0)}{P_{S|X}(s_i|1)} > \\
& \quad \frac{P_{L|X}(l'|0)}{P_{L|X}(l'|1)} \prod_{i=1}^{\dim(\mathbf{s}')} \frac{P_{S|X}(s'_i|0)}{P_{S|X}(s'_i|1)} \\
& \stackrel{(g)}{\Rightarrow} \Phi_v(l, \mathbf{s}) > \Phi_v(l', \mathbf{s}') \\
& \stackrel{(h)}{\Rightarrow} i < i',
\end{aligned} \quad (55)$$

where (f), (g) and (h) hold because of (9), (54), and (31), respectively.

(55) implies that elements in  $\mathcal{B}$  are listed in a way (see (31)) equivalent to listing  $(l, \mathbf{s}) \in \mathcal{L} \times \mathcal{S}^{d_v-1}$  in descending order based on  $P_{L,S|X}(l, \mathbf{s}|0)/P_{L,S|X}(l, \mathbf{s}|1)$  (see (2)). Therefore,  $Q_v$  defined by (35) can maximize  $I(X; R)$  among all the functions mapping  $\mathcal{L} \times \mathcal{S}^{d_v-1}$  to  $\mathcal{R}$  according to Section II-A.

#### ACKNOWLEDGMENT

This work is supported by SUTD SRG grant SRLS15095.

#### REFERENCES

- [1] R. G. Gallager, "Low-density parity-check codes," *IRE Trans. Inf. Theory*, vol. IT-8, no. 1, pp. 21–28, Jan. 1962.
- [2] J. Chen, A. Dholakia, E. Eleftheriou, M. P. Fossorier, and X.-Y. Hu, "Reduced-complexity decoding of LDPC codes," *IEEE Trans. Commun.*, vol. 53, no. 8, pp. 1288–1299, Aug. 2005.
- [3] D. Declercq, B. Vasic, S. K. Planjery, and E. Li, "Finite alphabet iterative decoders Part II: Towards guaranteed error correction of LDPC codes via iterative decoder diversity," *IEEE Trans. Commun.*, vol. 61, no. 10, pp. 4046–4057, Oct. 2013.
- [4] T. J. Richardson and R. L. Urbanke, "The capacity of low-density parity-check codes under message-passing decoding," *IEEE Trans. Inf. Theory*, vol. 47, no. 2, pp. 599–618, Feb. 2001.
- [5] J.-S. Lee and J. Thorpe, "Memory-efficient decoding of LDPC codes," in *Proc. IEEE Int. Symp. Inf. Theory*, Sep. 2005, pp. 459–463.
- [6] J. Thorpe, "Low-complexity approximations to belief propagation for LDPC codes," Oct. 2002. [Online]. Available: <http://www.systems.caltech.edu/~jeremy/research/papers/low-complexity.pdf>
- [7] B. M. Kurkoski, K. Yamaguchi, and K. Kobayashi, "Noise thresholds for discrete LDPC decoding mappings," in *Proc. IEEE Global Commun. Conf.*, Dec. 2008, pp. 1–5.
- [8] F. J. C. Romero and B. M. Kurkoski, "Decoding LDPC codes with mutual information-maximizing lookup tables," in *Proc. IEEE Int. Symp. Inf. Theory*, Jun. 2015, pp. 426–430.
- [9] —, "LDPC decoding mappings that maximize mutual information," *IEEE J. Sel. Areas Commun.*, vol. 34, no. 9, pp. 2391–2401, Sep. 2016.
- [10] J. Lewandowsky, M. Stark, and G. Bauch, "Optimum message mapping LDPC decoders derived from the sum-product algorithm," in *Proc. IEEE Int. Conf. Commun.*, May 2016, pp. 1–6.
- [11] J. Lewandowsky and G. Bauch, "Information-optimum LDPC decoders based on the information bottleneck method," *IEEE Access*, vol. 6, pp. 4054–4071, Jan. 2018.
- [12] M. Meidlinger, A. Balatsoukas-Stimming, A. Burg, and G. Matz, "Quantized message passing for LDPC codes," in *Proc. 49th Asilomar Conf. Signals, Syst., Comput.*, Nov. 2015, pp. 1606–1610.
- [13] M. Meidlinger and G. Matz, "On irregular LDPC codes with quantized message passing decoding," in *Proc. IEEE 18th Int. Workshop on Signal Processing Advances in Wireless Commun.*, Jul. 2017, pp. 1–5.
- [14] M. Stark, J. Lewandowsky, and G. Bauch, "Information-optimum LDPC decoders with message alignment for irregular codes," in *Proc. IEEE Global Commun. Conf.*, Dec. 2018, pp. 1–6.
- [15] B. M. Kurkoski and H. Yagi, "Quantization of binary-input discrete memoryless channels," *IEEE Trans. Inf. Theory*, vol. 60, no. 8, pp. 4544–4552, Aug. 2014.
- [16] X. He, K. Cai, W. Song, and Z. Mei, "Dynamic programming for discrete memoryless channel quantization," *arXiv*, Jan. 2019. [Online]. Available: <https://arxiv.org/abs/1901.01659>
- [17] T. H. Cormen, C. E. Leiserson, R. L. Rivest, and C. Stein, *Introduction to Algorithms: 2nd Edition*. Cambridge, MA, USA: MIT Press, 2001.
- [18] S.-Y. Chung, G. D. Forney, Jr., T. J. Richardson, and R. L. Urbanke, "On the design of low-density parity-check codes within 0.0045 dB of the Shannon limit," *IEEE Commun. Lett.*, vol. 5, no. 2, pp. 58–60, Feb. 2001.
- [19] K. Price, R. M. Storn, and J. A. Lampinen, *Differential evolution: a practical approach to global optimization*. Springer Science & Business Media, 2006.
- [20] K. Iwata and S. Ozawa, "Quantizer design for outputs of binary-input discrete memoryless channels using SMAWK algorithm," in *Proc. IEEE Int. Symp. Inf. Theory*, Jun. 2014, pp. 191–195.
- [21] J. Lewandowsky, G. Bauch, M. Tschauner, and P. Oppermann, "Design and evaluation of information bottleneck LDPC decoders for digital signal processors," *To be published in IEICE Trans. Commun.*, 2019.
- [22] *IEEE standard for information technology—telecommunications and information exchange between systems—local and metropolitan area networks—specific requirements part 3: Carrier sense multiple access with collision detection (CSMA/CD) access method and physical layer specifications*, IEEE Std. 802.3an, Sep. 2006.
- [23] D. J. C. MacKay, *Encyclopedia of sparse graph codes*. [Online]. Available: <http://www.inference.phy.cam.ac.uk/mackay/codes/data.html>
- [24] X. He, L. Zhou, and J. Du, "PEG-like design of binary QC-LDPC codes based on detecting and avoiding generating small cycles," *IEEE Trans. Commun.*, vol. 66, no. 5, pp. 1845–1858, May 2018.